Native Crystalline Polysaccharide Nanofibers: Processing and Properties

8

Pieter Samyn and Anayancy Osorio-Madrazo

Contents

Abstract

Native polysaccharide nanocrystals have gained increasing interest as fibrous reinforcement in nanocomposites. Unique mechanical properties combined with biodegradability and renewability have placed them as alternative for designing

P. Samyn (✉)
Applied and Analytical Chemistry, Institute for Materials Research (IMO-IMOMEC), Hasselt University, Diepenbeek, Belgium
e-mail: pieter.samyn@uhasselt.be

A. Osorio-Madrazo (✉)
Institute of Microsystems Engineering IMTEK – Laboratory for Sensors, and Freiburg Materials Research Center FMF, University of Freiburg, Freiburg, Germany
e-mail: anayancy.osorio@imtek.uni-freiburg.de

© Springer Nature Switzerland AG 2019

A. Barhoum et al. (eds.), *Handbook of Nanofibers*,
https://doi.org/10.1007/978-3-319-53655-2_17

environmentally friendly materials. The source origin and processing have a large impact on the nanofiber dimensions and properties. Most of the studies have been devoted to cellulose and chitin nanocrystals which are organized into fiber bundles in nature. Cellulose nanofibers can be obtained from animal, bacterial, algal, and plant sources. Chitin fibrils constitute, for example, fungal cell walls and arthropod exoskeletons. Based on processing, one defines two major families of polysaccharide nanofibers (whiskers and nanofibrils of polysaccharide). The preparation of the elementary whisker monocrystals has been achieved by acid hydrolysis, which allows collecting them after cleavage of the amorphous domains of the original substrates. Alternatively, the nanofibrillated material constitutes the other family, which results from the peeling of native microfibrils into a network of nanofibrils. The microfibril delamination is often performed with mechanical devices. Chitosan is the deacetylated derivative of chitin. Nevertheless, the preparation of chitosan crystalline nanofibrils that preserve the native directional packing is challenging. The preparation of chitosan nanofibril networks was recently reported by means of a chitosan mild hydrolysis at the solid state. This chapter reviews the methodologies used to produce crystalline nanofibers of polysaccharide with preserved native structural packing. Nanofibers of polysaccharides cellulose, chitin, and chitosan will be the focus of this review. The methods used to characterize these nanofibers will be revised, and the nanofiber properties will be discussed.

Keywords
Polysaccharide nanocrystals · Nanofibers · Cellulose · Chitin · Chitosan · Crystalline structure · Nanocomposites

Introduction

Nanocrystals from polysaccharides have gained increasing interest as stiff and fibrous reinforcing elements. Unique mechanical properties combined with biodegradability and natural renewability have placed polysaccharide nanofibers as an alternative of choice for designing environmentally friendly materials with enhanced performance. These nanocrystals are attracting great interest for their use as nanofillers in nanocomposites, relying on their exceptional potential to act as mechanical reinforcement or provide good barrier resistance. These properties are the result of the high crystallinity of the fibers resulting in almost defect-free crystalline structures and unique morphology with high aspect ratio forming an intertwined fiber network. In view of the design of more sustainable materials, it is evident that the crystalline polysaccharide fibers have become of broad interest.

Both cellulose and chitin form the most prevalent sources of natural polymers in Earth, both of them being examples of polysaccharides. The possibility for valorization of biomass residues into highly functional materials and the recyclability of the composite materials have brought the polysaccharide nanofibers to the forefront

of academic interest. In parallel, the first industrial production plants for cellulose nanofibers became operational since recent years with capacities ranging up to about 20 tons per day. The performance and inherent properties of the native fibers may strongly differ depending on the source composition, morphology, and functionality. The microstructures of naturally grown cellulose and chitin originate from the biosynthesis mechanism and are inevitably influenced by the environment. The hierarchical structure of native fibers, consisting of an arrangement of elementary fibers and fibrillar structures, allows breaking them down into nanoscale components by combined chemical and mechanical approaches. Thus, the source origin and processing have a large impact on the obtained polysaccharide nanofiber dimensions and properties. Many investigations describe the preparation of cellulose and chitin whisker nanocrystals by heterogeneous acid hydrolysis. Cellulose nanofibers can be obtained from animal, bacterial, algal, and plant sources. In the case of chitin, its main source is the cuticle of crustaceans, in which chitin is organized into fiber bundles. Similar to cellulose, chitin nanocrystals can be obtained by hydrolysis of chitin substrates with strong acid. Chitosan is the deacetylated derivative of chitin and is mainly produced by deacetylation of this latter in heterogeneous conditions. In the case of chitosan, the preparation of highly crystalline nanofibers with preserved native structural packing and high fiber length/width aspect ratio is challenging. Nevertheless, the preparation of nanofibrillated chitosan with preserved structural packing was recently reported, in which chitosan nanofibril networks were obtained by chitosan mild acid hydrolysis.

In order to improve the efficient use of polysaccharide nanofibers in various applications, a good comprehension of the relationship between natural occurrence, structure and physical/chemical properties is needed. Besides their origin, the latter are strongly influenced by the various processing routes, which often need to be optimized and tuned to become economically more feasible. Therefore, this chapter will review the methodologies used to produce crystalline nanofibers of polysaccharide with preserved native structural packing. Nanofibers of polysaccharides cellulose, chitin, and chitosan will be the focus of this review. The methods used to characterize this type of nanofibers will be revised, and the intrinsic nanofiber properties will be discussed.

Crystalline Directional Packing of Polysaccharide Nanofibers in Nature

Cellulose is a linear homopolymer of β(1→4)-linked units of D-glucopyranose biosynthesized by terrestrial and aquatic plants, animals, bacteria, and some amoebas. In the native cellulosic materials, the microfibril arrangement of cellulose stems from the biosynthesis mechanism and influences the cellulose nanofiber morphology. Cellulose chains arrange in a parallel fashion and their interaction leads to the formation of a highly crystalline structure. However, besides the crystalline regions (in general 40–70%) native cellulose contains amorphous domains whose proportion depends on the source. Specially, algal native cellulose can present a very high crystallinity of around 70%. Cellulose crystals of DP as high as 23000 are produced

by certain algae [1]. In the crystalline structure of native cellulose, linear chains are rigidified by intramolecular hydrogen bonds and these chains also interact with other ones to form a regular crystalline structure of cellulose I allomorph. Cellulose microfibril lengths can reach tens of microns. In the cellulose from the sea animal *Halocynthia roretzi*, called tunicin, cellulose microfibrils are highly crystalline as revealed by electron microscopy and diffraction studies [2]. Each microfibril often corresponds to a single crystal of about 10 nm in diameter. Besides, the microfibrils have a specific orientation in the tunicin and reveal a liquid crystal arrangement. The *Acetobacter* cellulose also has different levels of organization described as follows: the chains crystallize in the form of microfibrils, the hydrogen bonds between microfibrils produce bundles, and these bundles form ribbons. Each microfibril has a diameter of 3.0–3.5 nm, and approximately 50–80 microfibrils form ribbons of 40–60 nm in diameter.

Actually, native cellulose microfibrils can present two crystalline forms, namely, Iα and Iβ. The cellulose Iα is present in the cell walls of some algae and bacteria, while the cellulose Iβ is predominantly present in terrestrial plants, for example, in cotton, wood and ramie fibers [3]. Using X-ray and neutron crystallographic techniques, Nishiyama et al. [4] determined the crystal structures and hydrogen bond arrangements in both allomorphs at atomic resolution (1 Å). Cellulose Iα corresponds to a triclinic P_1 unit cell with one chain that has two neighboring glucose residues that are connected through a pseudo-twofold screw-axis symmetry (Fig. 1). Cellulose Iβ consists of a monoclinic $P2_1$ unit cell with two distinct chains of different conformations forming the so-called corner and center chains. Each cellulose Iβ chain has a twofold screw axis with the same adjacent glucosyl residues (Fig. 1). The structures of flat sheets that are held together by H-bonds are formed by the parallel up and edge-to-edge arrangements of the cellulose chains in both allomorphs. The major difference between cellulose Iα and cellulose Iβ is the pattern of the stagger of these sheets in the chain direction. The intrachain H-bond is formed by the interaction of the O3 secondary alcohol group of each residue donating its proton to the O5 ring atom of a neighboring residue. The groups of the O2 secondary alcohol and the O6 hydroxymethyl are both involved in the formation of an intra- and interchain H-bonding within the sheets. Further insight into the nature of H-bonding in cellulose Iβ was gained through neutron diffraction and quantum mechanics calculations, which allowed drawing two mutually exclusive H-bonding networks on the basis of the alternative locations for the protons of the center chain [5]. The unit cell parameters for crystalline cellulose allomorphs are summarized in Table 1.

Chitin is a linear polysaccharide of β(1→4)-linked units of 2-acetamido-2-deoxy-D-glucopyranose. The chitin occurs in the fungal cell walls and arthropod exoskeletons (e.g., of insects, crustaceans), or it is alternatively produced by marine algae (e.g., haptopheceaen, *Phaeocystis*, a centric diatom such as *Thalassiosira*) [7]. In parallel with the structure of cellulose, the native occurrence of chitin consists of a fibrous crystalline state like microfibrils. The main polymorphs of chitin are recognized as α-chitin and β-chitin depending on the differences in crystalline structures [8]. Chitin nanofibrils in arthropod cuticles are organized into helical structures displaying a cholesteric pattern [9]. The chitin microfibrillar arrangement (Fig. 2) is

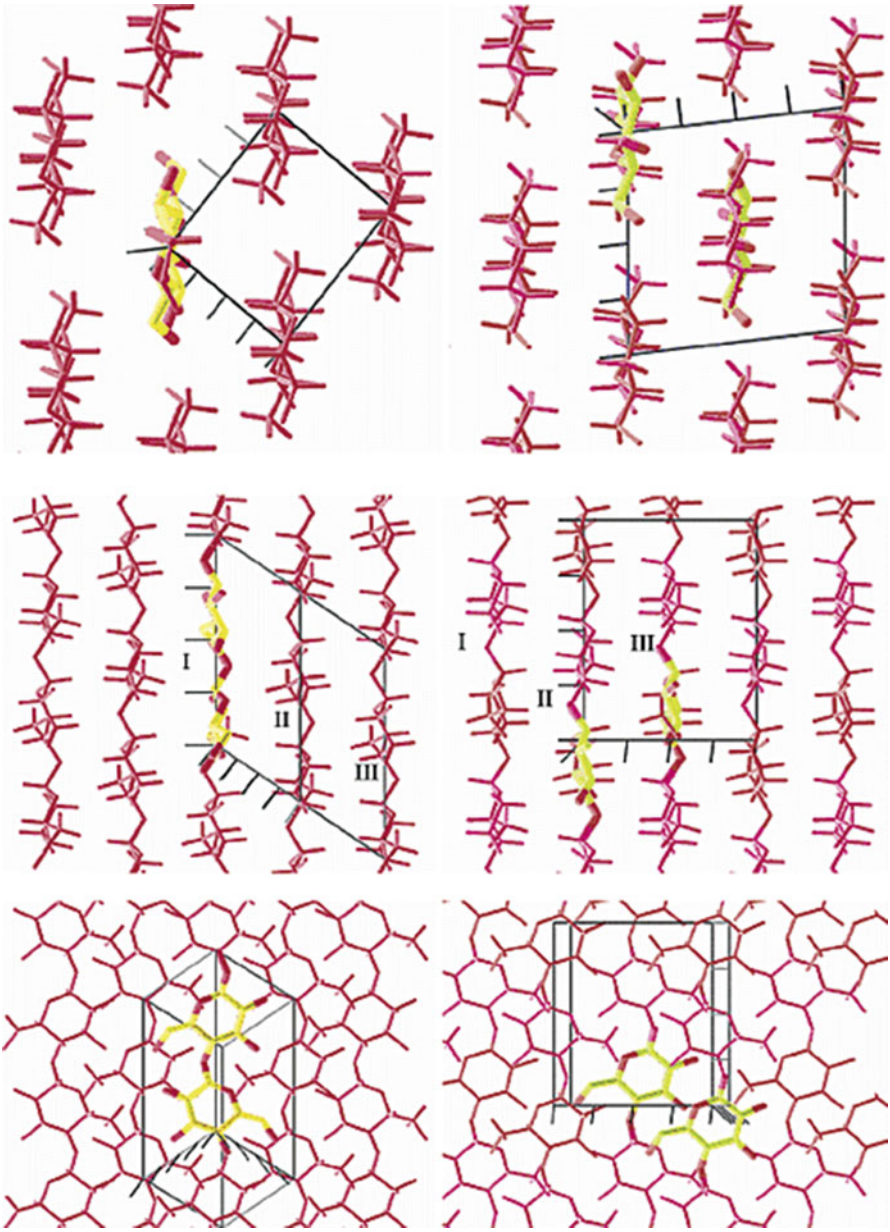

Fig. 1 Projections of the crystal structures of cellulose Iα (left) and cellulose Iβ (right) along different directions [6]

Table 1 Unit cell parameters of native cellulose I allomorphs

			Unit cell					
Type	Space group	Number of chains	a (Å)	b (Å)	c (Å)	α (°)	β (°)	γ (°)
Cellulose Iα	P_1	1	6.717	5.962	10.40	118.08	114.80	80.37
Cellulose Iβ	$P2_1$	2	7.784	8.201	10.38	90	90	96.55

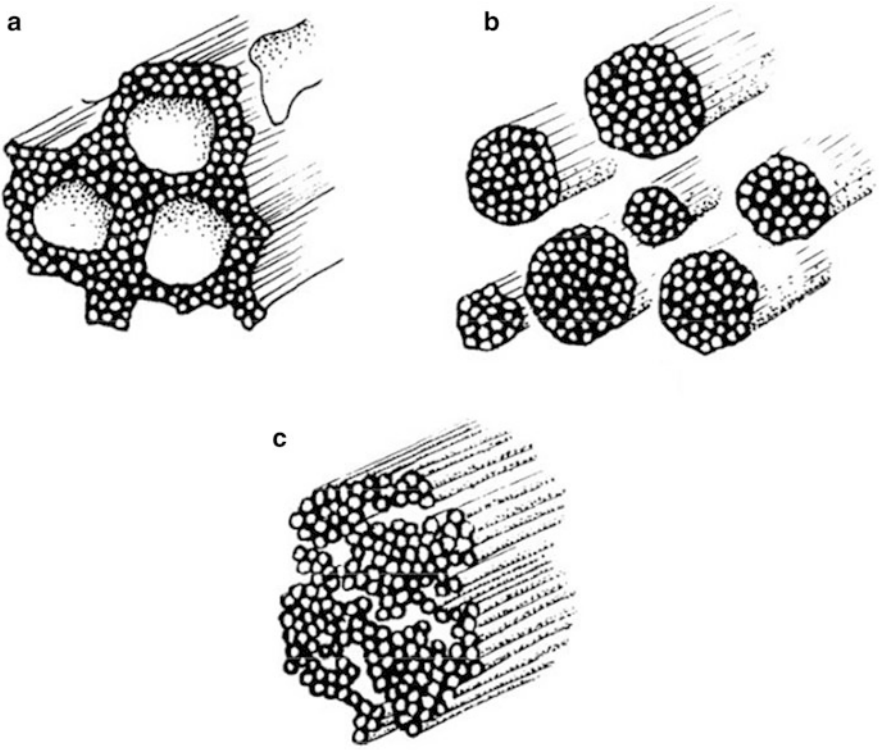

Fig. 2 Arrangements of the chitin-protein complex in the crab cuticle. Pre-ecdysial layers: (**a**) cross-linked structure in the lower layer of the pigment layer. Post-ecdysial layers: (**b**) association of microfibrils as fibrils in the main layer. (**c**) Homogeneous distribution of microfibrils in the membrane layer [11]

described by intramolecular hydrogen bonds similar to cellulose I. A protein sheath covers the crystalline microfibrils of chitin, mainly playing the role of lower modulus matrix in the chitin-protein complex. In general, the proteins do not penetrate the chitin crystallites, and the latter often form a hexagonal pseudo-array. The diameter of the chitin crystallites is of about 2.5–3.0 nm [10]. In crustacean cuticles, the chitin nanofibril assembly can lead to fiber bundles with diameters as large as 25 nm.

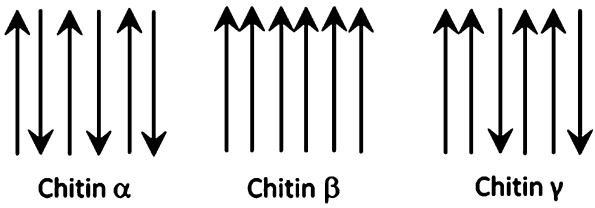

Fig. 3 Arrangement of chitin chains in the same sheet for the α-, β-, and γ-chitin allomorphs

Besides α- and β-chitin allomorphs, a third γ-chitin allomorph has been proposed. It is the sequence of chains (parallel or antiparallel arrangement) within a single sheet which will distinguish one allomorph from another as described in Fig. 3. Even if the three allomorphs can be found in the same animal, the α- and β-chitin are mainly found in the exoskeletons of crustaceans and in the endoskeletons of cephalopods, respectively. In the crystalline lattice, the chains are in the form of a helix 2_1, whatever the studied allomorph.

Processing of Crystalline Polysaccharide Nanofibers

One generally defines two major families of polysaccharide nanofibers based on how native polysaccharide microfibrils are processed [12]. Slender rodlike nanocrystals, coined polysaccharide nanowhiskers (CNW) or polysaccharide nanocrystals, represent one of these families, which are mainly obtained by hydrolysis of the polysaccharide substrate. Nanofibrillated polysaccharides, especially microfibrillated cellulose (MFC)/nanofibrillated cellulose (NFC) and nanofibrillated chitin, are another large family of polysaccharide nanofibers. They result from the shearing of the native microfibrils into an entangled network of nanofibers with a broad range of sizes displaying a hairy morphology. The delamination of the microfibril bundles through shearing is often done with mechanical devices such as high-pressure homogenizer or microfluidizers, although alternative methods such as cryo-crushing, refining, and ultrasonication have been reported.

Chemical Hydrolysis

Cellulose crystallites were isolated for the first time by chemical treatment of a cotton substrate in hot concentrated sulfuric acid in the late 1940s. Thus, the amorphous regions of native polysaccharide microfibrils can be hydrolyzed in general with strong acid, liberating the elementary monocrystals. The colloidal stability of the nanocellulose crystals can be governed by electrostatic repulsion due to the charges at the surface induced through the chemical reaction of sulfuric acid with hydroxyl groups at the surface and consequent formation of sulfate ester groups [13]. In parallel with the introduction of surface charges, the cellulose nanocrystals are able to form a liquid crystalline phase through self-organization.

The cellulose nanowhiskers (CNWs) are commonly obtained by chemical acid hydrolysis of pulp fibers or microcrystalline cellulose (MCC) in combination with a sonication treatment, using sulfuric, hydrochloric, or phosphoric acid. Crystalline nanoparticles resulting from the sulfuric acid hydrolysis of cellulose from cotton, Avicel, and tunicate were obtained by Elazzouzi-Hafraoui et al. [14], where the majority of the obtained cellulose particles were flat objects constituted by elementary crystallites whose lateral adhesion was resistant against hydrolysis and sonication treatments.

Both the substrate origin and the hydrolysis parameters play an important role on the final dimensions of the polysaccharide nanofibers. The geometry of the CNWs can be controlled by varying the hydrolysis parameters, such as temperature (e.g., 20, 40, and 60 °C), time (e.g., 2, 4, and 6 h), and acid concentration (e.g., 20, 40, and 60 wt%). The combination of a hydrolysis reaction and high-pressure homogenization resulted in nanoparticles with a diameter of 11–33 nm and a length of 199–344 nm. A good monitoring of the process allows optimization to ensure maximum yield and purity, characterized by high crystallinity and narrow size distribution. Many studies describe the preparation of cellulose [15] and chitin crystalline nanofibers [16] by heterogeneous acid hydrolysis. A number of investigations concerning the preparation of cellulose nanocrystals have been reported. After diffusion of acid within the substrate, the glycosidic bonds of cellulose polymer chain in the disordered regions, more accessible and reactive, are preferentially broken. The selective acid cleavage of the glycosidic bonds is attributed to the differences in the kinetics of hydrolysis for the amorphous and crystalline domains. This process generally results in a rapid decrease in degree of polymerization (DP) of the carbohydrate polymer molecules toward a constant level-off DP (LODP) with values depending on the substrate origin, while the crystallinity of the remaining particles increases [17]. Cellulose whisker nanocrystals as shown in Fig. 4 have been produced from different sources.

The CNWs could be produced in yields from 20% to 40% in a concentrated acid environment, while lower yields have been obtained in diluted acid. Relatively high yields of about 48% could be obtained in mildly acidic aqueous ionic liquids [19]. The higher efficiency of the hydrolysis reaction could be attributed to the lower solvating power of an aqueous ionic liquid in contrast with a concentrated sulfuric acid. After optimization of a two-step hydrolysis with mildly acidic ionic liquid (IL) 1-buty1-3-methylimidazolium hydrogen sulfate, CNWs were produced in near theoretical yield levels from bleached softwood kraft pulp, bleached hardwood kraft pulp, and microcrystalline cellulose. This technique also allows to extract CNWs directly from lignocellulosic biomass, by simultaneously delignifying, defibrillating, hydrolyzing, and derivatizing the cellulose from wood [20]. This method was also used in combination with steam explosion as a pretreatment to enhance lignocellulose accessibility [21]. This direct route of extraction of nanofibers, with dimensions close to their native state in wood, allows easy processing without the need of purification/dialysis compared to traditional routes. The use of IL allows to create modified CNWs that can be directly used, for example, as metal-free catalysts for nanostructured materials [22].

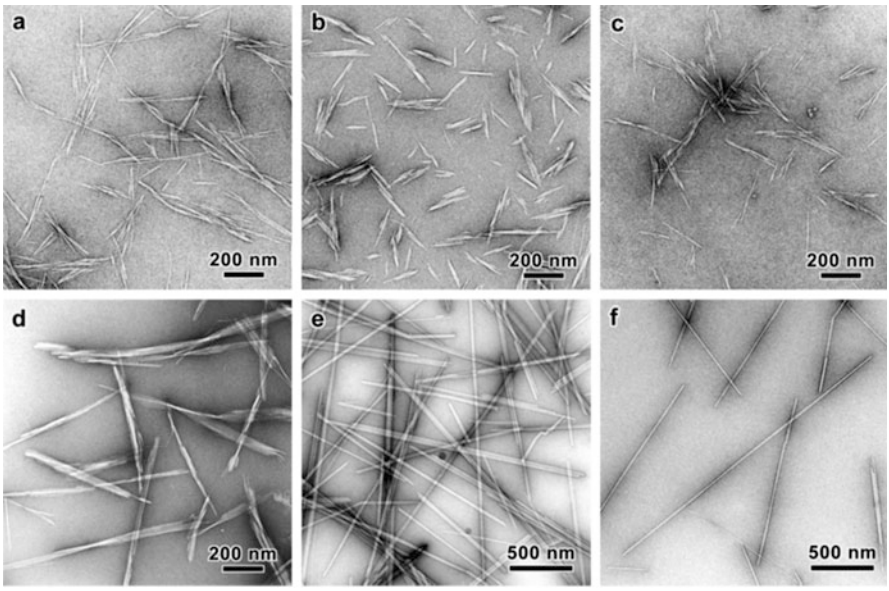

Fig. 4 TEM images of negatively stained preparations of CNCs of various origins: (**a**) wood (Courtesy of G. Chauve, FPInnovations); (**b**) cotton (Courtesy of F. Azzam, CERMAV); (**c**) bamboo (Courtesy B. Jean, CERMAV; (**d**) *Gluconacetobacter xylinus* (Courtesy of H. Bizot, INRA); (**e**) *Glaucocystis* (Courtesy of Y. Nishiyama, CERMAV); (**f**) *Halocynthia papillosa* (Courtesy of A. Osorio-Madrazo, IMTEK/FMF University of Freiburg) [18]

By analogy with cellulose, the acid hydrolysis of chitin produces a suspension of whiskers showing a cholesteric liquid crystalline phase above a certain concentration. The chitinous substrate is boiled and stirred in an aqueous KOH solution to remove the residual proteins. Suspensions of chitin crystallites are then prepared by acid hydrolysis in order to dissolve the regions with a low lateral structural order. In that way, the highly crystalline residue remains insoluble, and the aid of mechanical shearing finally converts the chitin whiskers into a stable suspension. The preparation of highly crystalline chitosan (CHI) nanofibrils that preserve the native directional packing and macromolecular structure is challenging. The acid hydrolysis has been also reported as a method to increase crystallinity of CHI substrates [23]. There have been trials for the production of CHI nanofibers by the deacetylation of chitin nanowhiskers, but it neither results in a needlelike structure of CHI nanowhiskers nor in a network of crystalline nanofibrils. Indeed, the deacetylation of chitin whiskers yields CHI scaffolds with a significant loss of crystallinity. By deacetylating chitin whiskers in $NaOH/NaBH_4$ [24], the CHI nanoparticles did not resemble whiskers as they presented a very low aspect ratio (L/d ~4.8), which is significantly lower than the aspect ratios reported for chitin and cellulose whiskers (L/d 20–130) [25]. In fact, the obtained nanoparticles should be referred to as chitin whiskers rather than chitosan, as the degree of N-acetylation (*DA*) remained as high as 50% after the deacetylation reaction. It was also revealed that a long deacetylation

of chitin whiskers compromises the integrity of the fibrillar morphology. Most of the studies on CHI crystals have been performed on previously solubilized oligomers (e.g., *DP* ~35), losing the native packing [26]. The preparation of CHI nanofibrils, preserving both the native structural packing and polymer high molecular weight, was recently reported [27].

Mechanical Grinding and Fibrillation

Due to the hierarchical arrangement of cellulose fibers within the wood structure with alignment in the secondary cell wall and organization of microfibrils and elementary fibrils within the bundle of fibers, the latter can be separated under mechanically induced shear action. Therefore, the cellulose microfibril (CMF) or cellulose nanofibril (CNF) can be produced by isolation of the fibrils through mechanical processes such as grinding, cryo-crushing, or high-pressure homogenization. After processing, the CMF or CNF is composed of both amorphous and crystalline domains, while the degree of polymerization (DP) of the original cellulose molecules is only slightly reduced without severe cleavage of the cellulose polymer chains. When an original fiber suspension is grinded between a rotating and a stationary disc, the disintegration of the fibers into the microfibrillar components occurs. With adapting the configuration of the grooves in the discs consisting of resin and wear-resistant silicon carbide materials, the flow of the fibers can be guided, and different fines can be produced. The main advantage of processing with the micro-grinder is that the mechanical fiber shortening pretreatment utilized with other processing techniques may not be required. Another production route by cryo-crushing starts with freezing the water present in the pulp suspension followed by the release of fibrils under high impact load. However, the cryo-crushing mostly is used to produce cellulose fibrils within the micron size originating from primary cell walls, while it is not suited to obtain very thin fibrils [28]. For the latter, more intensive processing is required under homogenization, where a suspension of wood or cellulose fibers is circulated through a homogenization chamber with sharp pressure drops inducing high impact forces. The latter is used to induce high internal shear forces in the fiber structure, thereby splitting the cellulose fibers into micro- or nanofiber components. For example, the circulation over 10–20 passes with a pressure drop of about 55 MPa typically results in microfibrillated cellulose (MFC), containing fibers with 100 nm to 1 μm diameter and a few hundred microns to maximum 1 mm in length. The more severe processing steps using 5–20 passes combined with pressures of 55–210 MPa typically results in nanofibrillated cellulose (NFC) with the smaller diameters of 10–100 nm and the length from few hundred nanometers to some microns. The finally obtained fiber suspensions often contain a mixture of fibers with different morphologies that can be categorized as both MFC and NFC. With increasing the number of processing steps, the geometry of fibers in a MFC suspension remains less homogeneous than NFC suspensions. In order to obtain better defined and controlled geometries, the production of MFC is mainly performed by a single-step mechanical treatment of native pulp, while the NFC is

produced in combination of a chemical pretreatment and mechanical treatment [29]. However, the processing of pulp suspensions by mechanical fibrillation requires enormously high amounts of energy varying along the different processing equipment. An indication of the energy consumption to produce MFC bleached and unbleached wood pulp fibers by homogenization, microfluidization, and micro-grinding, is summarized in Table 2 [30].

Similarly, chitin nanofibers forming a dense and uniform nanofiber network have been prepared by fibrillation using a grinding technique. The chitin nanofibers can be obtained from different origins including crab shell, prawn shell, mushroom, and dried chitin powders and are consequently endowed with specific properties [31]. In the case of chitin, the mechanical treatment under acidic conditions is the most favorable route, as the cationization of amino groups on the chitin fiber facilitates fibrillation into nanofibers by electrostatic repulsions. The purification of the chitin powders and adjustment of the pH with acidic acid are critical steps in the fibrillation process. In particular, the cationization of the C2 amino groups on the chitin fiber surface at pH between 3 and 4 is required to maintain the stable dispersion state by electrostatic repulsions to prevent coacervation [32]. A 2,2,6,6-tetra-methylpiperidine-1-oxyl (TEMPO) radical oxidation is performed at high pH followed by addition of HCl to reach the lower pH. Following another acidic route, the phosphoric acid was used, and different morphologies of chitin nanofibers could be obtained depending on the dissolution time and temperature. As an alternative more direct route, the chitin nanofibers could be prepared directly from prawn shell by grinding under neutral pH conditions after removal of proteins and minerals [33], and the fiber morphologies are comparable to the properties of fibrils

Table 2 Energy consumption for production of MFC (Adapted from [30])

Processing method	Pretreatment	Pressure or speed	Number of passes	Total energy consumption (kJ/kg)
Micro-grinder	–	1500 rpm	9	5580
	V. Beater	1500 rpm	9	12,810
Homogenizer	V. Beater	55 MPa	20	78,800
Microfluidizer M-110 P	V. Beater	69 MPa	1 (H210Z)	8430
		69 MPa	5 (G10Z)	
	V. Beater	69 MPa	5 (H210Z)	10,180
		138 MPa	5 (G10Z)	
	V. Beater	69 MPa	20 (H210Z)	11,230
Microfluidizer M-110 EH	V. Beater	69 MPa	1 (H210Z)	
		207 MPa	5 (G10Z)	10,580
	V. Beater	69 MPa	1 (H210Z)	8430
		69 MPa	5 (G10Z)	
	V. Beater	69 MPa	20 (H210Z)	11,230
	V. Beater	207 MPa	5 (G10Z)	10,380
	V. Beater	138 MPa	5 (G10Z)	9180
	V. Beater	69 MPa	5 (G10Z)	8230

obtained from crab shell treated under acidic pH. The nanofibers presented uniform morphology with 10–20 nm width and high aspect ratios. In other mild approaches, an ultrasound process is used to transform crab shells into completely fibrillated chitin nanofibers, where the α-chitin crystalline structure is almost preserved while processing in parallel with high purity and low degree of deacetylation below 15%. Special attention to the effects of surface charges on processing of the nanofibers has been considered, by comparing the production from partially deacetylated and TEMPO-mediated oxidized α-chitin, where the partially deacetylated fibers resulted in smaller diameters and higher thermal resistance [34].

Effects of Pretreatment

The enzymatic pretreatments are used for the local removal or modification of the lignin and hemicellulose parts without directly affecting the cellulose fibers. Different types of enzymes can be traditionally used, including the so-called cellobiohydrolases (A- and B-type cellulases) that have most effects on the attack of the crystalline cellulose or otherwise the endoglucanases (C- and D-type cellulases) that do not degrade that native cellulose structure. Under mild enzymatic conditions, the pretreatment has also been directly combined with the refining or homogenization of NFC into homogeneous fiber dispersion. The mild enzymatic reactions resulted in fibers with a higher aspect ratio, and their effects were less drastic compared to a more aggressive acid hydrolysis [35].

The alkaline-acid pretreatments result in the solubilization of lignin, hemicellulose, and pectin. In the first phase, the fibers are soaked in a solution of sodium hydroxide to increase the surface of the cellulose fibers in order to become more sensitive to the subsequent hydrolysis. In the second phase, the fibers are hydrolyzed with hydrochloric acid at 60–80 °C in order to solubilize the hemicelluloses. Finally in the third phase, the fibers are processed with sodium hydroxide at 60–80 °C dissolving the lignin structure in parallel with the disruption of the linkage bonds between the carbohydrates and lignin. An alternative way comprises the pretreatment with alkaline peroxide to rapidly degrade the lignin compounds into low molecular weight products [36]. During these processes, however, the crystalline structure of the cellulose fibers may change: with higher extent and severity of the alkaline treatment, a transition from cellulose I to cellulose II structure results in fibers with lower mechanical properties. The severe acid hydrolysis of cellulose fibers in the presence of sulfuric acid may induce sulfated groups at the fiber surfaces, which lead to a lower thermal stability and different behavior of the fiber suspensions attributed to various fiber interactions.

Recently, the ionic liquids have been used as a pretreatment method before mechanical isolation of NFC: the pretreatment results in dissolving the cellulose and can be favorably applied before the high-pressure homogenization step. The chemistry of ionic liquids can be easily adapted to dissolve a wide variety of biomass: unlike the heterogeneous reaction environment in water, the ionic liquids make the catalytic sites highly access the β-glycosidic bonds, which facilitates the reaction of biomass fractionation and hydrolysis of cellulose [37].

Intrinsic Polysaccharide Nanofiber Properties

The nanometric features and chemistry of the processed polysaccharide nanofibers influence their properties such as morphology, crystalline microstructure, rheology of the nanofiber suspensions, threshold concentration for phase separation, liquid crystal behavior, preferred orientation under electric or magnetic field, mechanical behavior, and reinforcement capacity in nanocomposites.

Morphology and Crystalline Microstructure of Processed Nanofibers

The knowledge of the precise control over size and morphology of cellulose nanocrystals are important parameters that will affect the performance of the nanocellulose fibers and final product properties when applications are envisaged. The geometry and dimensions of rodlike cellulose nanocrystals highly depend on the selected source of cellulose (Table 3) and are further influenced by the conditions of the hydrolysis reaction. For example, the processed cellulose nanocrystals from wood can be 3–7 nm in width and 100–200 nm in length, while those derived from tunicate can be 10–20 nm in width and 500–2000 nm in length. This indicates how the different sources and reaction conditions result in different sizes and size distributions. This distribution may have an impact on the properties and applications of polysaccharide nanocrystals. Nevertheless, it is worth to notice that the state of individualization of the particles in the colloidal suspension is strongly affected by the nanoparticle concentration and external parameters such as pH, ionic strength, and temperature. The stabilization of the colloidal system with cellulose nanoparticles can be controlled by their surface chemistry, in particular the electrostatic repulsion forces provided by the negative charges at the surface due to the sulfate

Table 3 Size distribution of cellulose and chitin nanowhiskers from some different sources

Polysaccharide nanofiber and source	Length (nm)	Width	Aspect ratio
Cellulose nanowhiskers			
Sisal	100–200	3–7	~30
Ramie	50–250	5–10	~15
Rice	50–300	10–15	~12
Cotton	100–300	8–10	~20
Microcrystalline cellulose (MCC) from wood	50–500	5–50	~10
Tunicate	100–3000	10–50	~100
Algae *Cladophora*	200–4000	15–40	~150
Algae *Microdictyon tennis*	1000–10,000	25–35	~200
Bacteria	200–3000	10–75	~100
Chitin nanowhiskers			
Riftia tubes	500–10,000	18	~120
Squid pen	50–300	10	15
Crab shell	100–650	4–40	16

ester groups. The cross sections of polysaccharide nanocrystals also display different shapes, e.g., square, rectangular, or parallelogram, which are dictated by the arrangements of enzymatic terminal complexes extruding cellulose chains during the biosynthesis. Various techniques based on microscopy, light scattering, electrical properties, sedimentation, sorting, and classification allow access to particle size. The morphology of polysaccharide nanocrystals can be assessed by microscopic methods like field emission gun scanning electron microscopy (FEG-SEM), transmission electron microscopy (TEM), cryo-TEM, or atomic force microscopy (AFM). The light scattering techniques such as small- and wide-angle neutron or X-ray scattering (SANS, WANS, SAXS, and WAXS, respectively) give additional size and structural information.

The morphology of the fibrillated cellulose is determined by their aspect ratio typically in the range of L/d = 100 to 200 for MFC toward L/d = 200 to 400 for NFC. The morphology of the fibers may be described qualitatively or quantitatively by the fiber diameter, surface roughness, size distribution, or degree of fibrillation. The latter expresses the extent to which the fiber has partially been split longitudinally into thinner fibrils. Consequently, it increases the surface area and importantly influences the absorption properties, softness of the fiber, rheological properties, and interactions with a polymer matrix in composites. The morphology gradually changes with the processing sequence in the microfluidizer and corresponding diameter of the interaction chamber and/or number of passes. AFM images of fibrillated cellulose obtained from hardwood kraft pulp processed with gradually decreasing chamber size and increasing number of passes is shown in Fig. 5. It was observed that a higher number of subsequent processing passes, through the same type of interaction chamber, progressively reduces the maximum fiber diameter leading to a suspension with narrower distribution in fiber diameters. Finally, the minimum diameter of the fibrillated fibers was mainly influenced by the choice of the type of interaction chamber and did not vary significantly with a higher number of passes within the chamber [38].

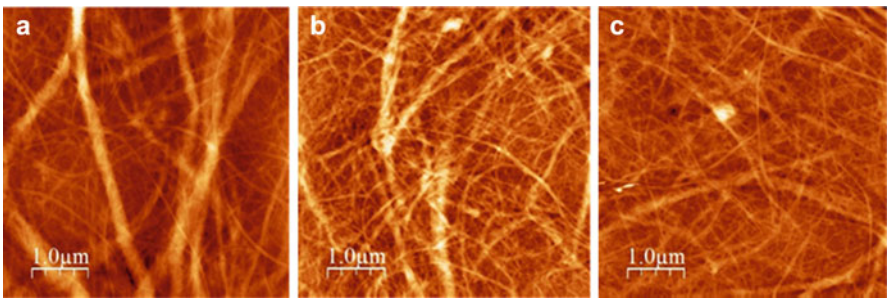

Fig. 5 Morphologies of fibrillated cellulose for different processing conditions in the microfluidizer EH-110, (**a**) 25 passes through homogenizer, (**b**) 10 additional passes in 200 μm chamber, (**c**) 10 additional passes in 87 μm chamber [38]

The degree of crystallinity of polysaccharide nanofibers can traditionally be determined from X-ray diffraction analysis. Alternatively, a crystallinity index can be also determined from Raman microscopy, as the intensity of peaks at 1462 and 1481 cm^{-1} corresponding to CH_2 bending, relates to amorphous and crystalline proportions in cellulosic sample, respectively [39]. The characterization of the intrinsic nanostructure of cellulose types originating from different resources can give better insight in the different properties and responses of these materials at the macroscale level, resulting in, for example, variations in mechanical properties or swelling. The crystallinity of the as above-processed crystalline polysaccharide nanofibers are similar to the initial microfibrils. In the case of cellulose, a microcrystal consists of contiguous crystalline blocks corresponding to cellulose I. After treatment by acid hydrolysis, the crystal integrity of the native fibers has generally been maintained with a progressive increase in crystallinity for raw bamboo fiber (47.91%), pulp (54.34%), bleached pulp (60.89%), and CNF (65.32%), respectively [40]. The latter is in consent with the dissolution and removal of components including lignin, hemicelluloses, and some other noncellulosic polysaccharides that are present in amorphous regions of the native cellulose fibers. It might also appear that the orientation of the cellulose molecular chains along particular directions increases. In some cases, however, it was described that the degree of crystallinity and size of the crystallites of cellulose may decrease after sulfuric acid hydrolysis, due to the more severe attack by the acid environment not only to the amorphous phases but also to the crystalline domains. This may be due to higher acid concentration where degradation of cellulose occurs and crystallinity decreases. Besides, the comparison of crystallinity between sulfuric acid-treated nanowhiskers and sulfuric acid-neutralized nanowhiskers did not reveal any differences, suggesting that the cellulose I structure is maintained after processing. An eventual reduction of crystallite sizes after acid hydrolysis can be attributed to a shortening of the crystalline domains. Otherwise, the sulfuric treatment can change the structure of cellulose I to cellulose II in comparison with the more mild treatment with HCl. By removing amorphous components, the hydroxyl groups on the cellulose surface could form new hydrogen bonds with consequent increasing crystallinity. The cellulose extractions from wheat straw via hydrochloric, nitric, and sulfuric acid hydrolysis methods revealed that the structure of the cellulose exhibited a mixture of cellulose I and cellulose III polymorphs depending on the acid conditions used. In particular, portions of the cellulose will swell and dissolve at sulfuric acid concentrations stronger than 63–64 wt.%, with the regenerated dissolved cellulose exhibiting a cellulose II polymorph structural arrangement at concentrations between 64 and 65 wt.%. Therefore, the insoluble cellulose exhibits a crystalline structure cellulose I, while the regenerated cellulose exhibits a crystalline polymorph cellulose II. Duchemin et al. [41] prepared all-cellulose materials consisting of crystallites of cellulose I dispersed in a paracrystalline and amorphous cellulose matrix by partial solubilization of the native cellulosic material (microcrystalline cellulose (MCC)) and further regeneration of the solubilized part. This combination of cellulose I crystallites embedded in a more disordered phase seems promising to achieve self-nanoreinforced materials of unique chemical structure. This methodology demonstrates

how the native crystalline packing of polysaccharide nanofibers can be used as self-template to produce single compound nanoreinforced materials. Kondo et al. [42] introduced the concept of "nematic ordered cellulose" to interpret intermediate states of molecular ordering, displaying features of each allomorph of the polysaccharide, yet not perfectly matching to any allomorph. Cellulose nanocrystals obtained from the algae *Cladophora* sp. have been investigated by TEM and synchrotron X-ray diffraction analysis. The TEM images and the X-ray synchrotron diffraction pattern of the whiskers are shown in Fig. 6 [25]. The whiskers consisted of extremely long needle-shaped single crystals with diffraction peaks indexed as the (100), (010), (002), (110), and ($\bar{1}\,\bar{1}\,4$) reflections of triclinic cellulose Iα allomorph.

The combination of neutron crystallography studies with ab initio quantum mechanics and empirical force field molecular dynamics revealed interesting results. The cellulose Iβ nanocrystals from hydrolyzed tunicin mostly consist of chains with a crystalline Iβ arrangement and H-bonding in one (so-called scheme A) of the two mutually H-bonding networks proposed for cellulose Iβ [5]. Then, smaller regions of static H-bond disorder exist, perhaps at defects within crystalline domains, at interfaces between crystalline domains or at the surfaces of the microfibril. The disruption of the interchain H-bond O2-H· · ·O6 observed in scheme A can cause the

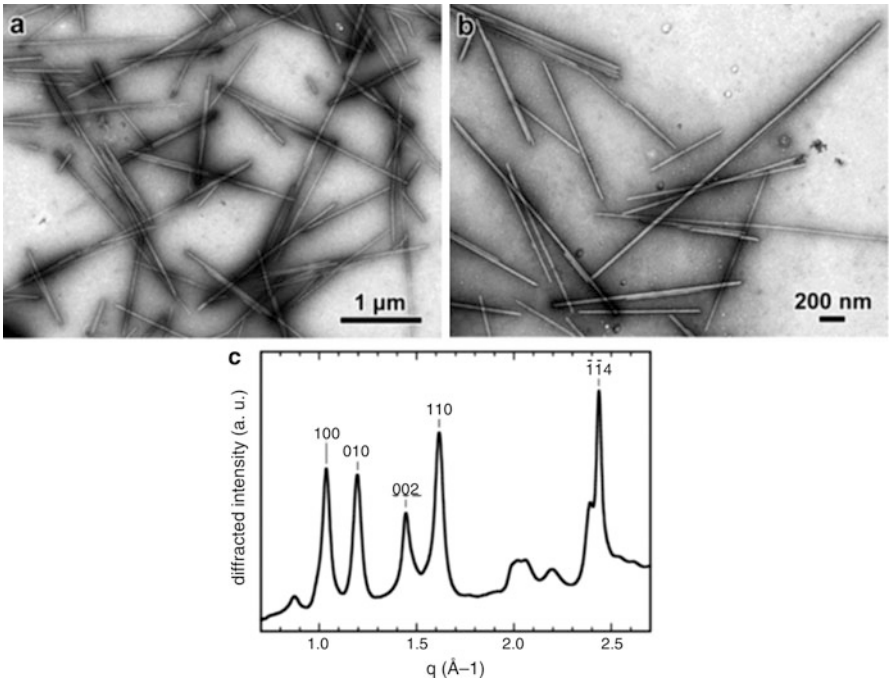

Fig. 6 (**a**, **b**) TEM images of negatively stained *Cladophora* cellulose whiskers; (**c**) wide-angle synchrotron X-ray diffraction profile from a pellet of *Cladophora* cellulose whiskers. The indexation of the main peaks corresponds to that of triclinic cellulose Iα allomorph [25]

destabilization of the dipole-dipole interactions between the O2-H and O3-H hydroxyl groups that favor the reorientation of O2-H so that it forms a three-bond cooperative network that is a feature of the second proposed H-bonding network, so-called scheme B. Although the experimental results were obtained with large nanocrystals of cellulose from hydrolyzed tunicin, they may be relevant for the understanding of some differences in the properties of cellulose microfibrils found in different naturally occurring systems. For different types of origins, the microfibrils may contain limited zones of the crystalline Iβ form next to other regions that consist of the crystalline Iα form and some zones with poorly ordered structure. Although the crystalline Iβ regions in microfibrils have mainly H-bonding according to scheme A, the H-bonding in scheme B may be more important to determine the properties at the surfaces and interfaces of the crystalline Iβ regions, in particular the chemical reactivity and sensitivity for degradation by enzymatic hydrolysis. Different states with more extensive disorder in the native microfibrillar packing may be more significant. The cellulose may contain two temperature regions that lead to either static or dynamic disorder, as well as an intermediate temperature range corresponding to a transition region between static and dynamic disorder [5].

For the micro-/nanofibrillated cellulose, there are findings of both increase and decrease in crystallinity. The decrease in crystallinity under pure high-pressure disintegration may happen [43]: this can be related to an alteration of crystallinity under high mechanical shear forces and consequent frictional forces on the crystalline regions. In some cases, the cleavage of the crystalline region is believed to play its role in the fibrillation of nanofibers and cellulose bundles [44]. In parallel with the crystallinity lowering, the degree of polymerization continuously decreases with ongoing fibrillation time during grinding (Fig. 7) [45]. The cellulose crystals are destroyed, and the chain length is subsequently shortened under continuous shearing by grinding discs, resulting in smaller crystal sizes and reduced crystallinity. Alternatively, some processing conditions also revealed an increase in crystallinity with ongoing fibrillation within a microfluidizer [38], which might be explained by a decrease in the random amorphous phase by orientation of smectic regions under shear. The pretreatments of alkalinization, oxidation by adding chlorine and

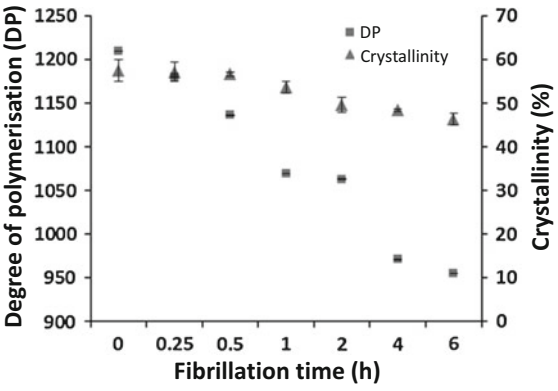

Fig. 7 Variation of the degree of polymerization and crystallinity with fibrillation time during production of microfibrillated cellulose [45]

hydrolysis by adding acid during fibrillation more likely result in efficient removal of the amorphous zones and increase in crystallinity [46].

Despite the aggressiveness of the reactions carried out during the extraction and purification of chitin and the deacetylation of chitin to obtain chitosan, the supramolecular fiber organization is preserved. Even during the hydrolysis of chitosan, the cholesteric organization of the fibers is preserved. The X-ray fiber diffraction pattern of the hydrated (tendon) polymorph of chitosan was explained on the basis of an orthorhombic unit cell with the following dimensions: $a = 8.95$, b = 16.97, and c (fiber axis) = 10.34 Å [47, 48]. The molecular structure in this crystalline form is characterized by a 2_1 helical symmetry, and the formation of O3...O5 hydrogen bonds is used for the stabilization of the conformation in the unit cell. The unit cell contains eight water molecules, consisting of two molecules in an asymmetric unit (1 H_2O/monosaccharide). A new polymorph was later suggested based on an energetically more stable structure with additional interchain hydrogen bonding formed upon removal of loosely bound water between chains along the [010] direction [49]. The annealed samples of chitosan have been prepared by heating in water at 200–220 °C [50]. The anhydrous chitosan has been also obtained by keeping a chitosan/acetic acid complex in 100% relative humidity (RH) for several days, at room temperature [51]. As a result, a well-preserved orientation and crystallinity have been detected from the X-ray diffraction pattern compared to those obtained by annealing, due to the mild annealing conditions. No direct interaction between successive sheets of polymer chains along the *a*-axis has been detected in the anhydrous polymorph. The chitosan molecules were characterized with a twofold helical symmetry, while the strong O3...O5 and weak O3...O6 hydrogen bonds help to stabilize the conformation in the unit cell within a repeat period of 10.43 Å.

The synchrotron WAXS patterns of starting chitosan flakes and processed nanofibril networks were analyzed [27]. Figure 8 shows radial averages of the 2D WAXS images of chitosan nanofibril networks. The pattern of the starting particles shows signals corresponding to reflections of chitosan hydrated allomorph (labeled with h) (Fig. 8a). This is the characteristic pattern of the hydrated allomorph described by Clark and Smith [47] and later on by Okuyama et al. [48]. The WAXS patterns of the nanofibril networks obtained after hydrolysis showed new reflections corresponding to the chitosan anhydrous allomorph (labeled with a) (Fig. 8b). For nanofibril networks obtained by multistep hydrolysis, peaks of the anhydrous allomorph were mainly observed. In addition to the typical anhydrous allomorph peaks at q = 1.00, 1.40, 1.58, 1.62, and 2.45°A^{-1}, the high-resolution synchrotron analysis allowed indexing other chitosan anhydrous allomorph reflections (Fig. 8b). The large contribution of diffraction reflections reveals the high crystallinity of the nanofibrils. The recrystallization into anhydrous allomorph was related to a higher mobility of the hydrolyzed chains in concentrated acid, in which conditions the hydrophobic interactions are favored.

Figure 9 shows electron diffraction diagrams of selected aligned chitosan nanofibril areas [27] revealing the fiber diffraction diagrams. For the patterns of the starting CHI particles, three equatorial reflections $(0\ 2\ 0)_h$, $(2\ 0\ 0)_h$, and $(2\ 2\ 0)_h$

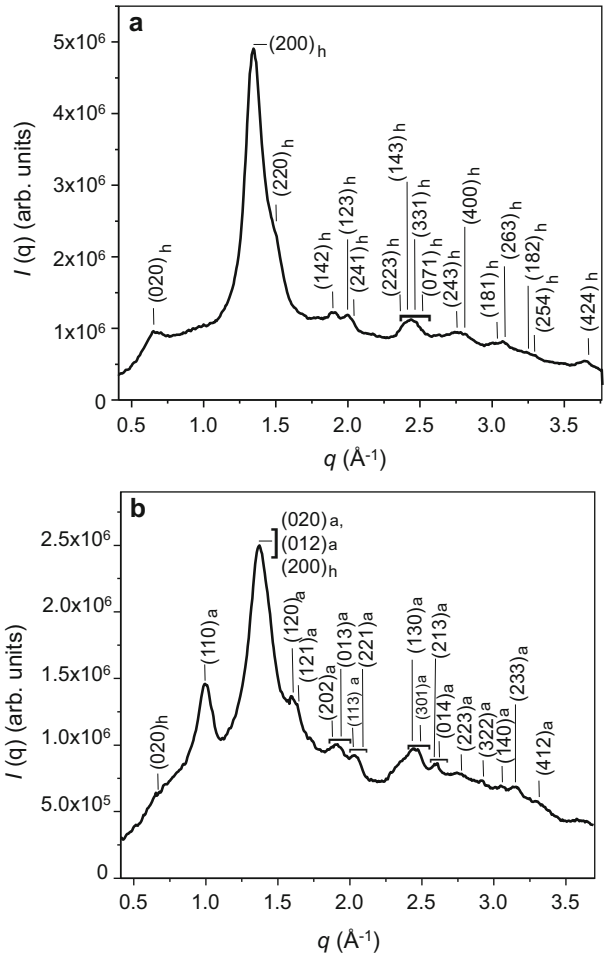

Fig. 8 Synchrotron WAXS radial averages of chitosan nanofibrils presenting different allomorph contributions: (**a**) mainly chitosan hydrated allomorph (h); (**b**) mainly anhydrous allomorph (**a**) [27]

are observed corresponding to the CHI hydrated allomorph (Fig. 9a). After single hydrolysis, the equatorial reflections of both hydrated and anhydrous allomorphs are visualized (Fig. 9b). Finally, the pattern of the nanofibril networks obtained by a multistep hydrolysis reaction with equatorial spots of $(1\ 1\ 0)_a$, $(0\ 2\ 0)_a$, and $(0\ 1\ 2)$ only showed the reflections corresponding to the CHI anhydrous allomorph (Fig. 9c). This supports the results from the WAXS analysis, i.e., the orientation during the development of the anhydrous crystals remains similar to that of the parent hydrated crystals present in the starting fibrils. It also supports the suggestion that the nanofibril networks are constituted by crystallites with the same alignment of their native material, i.e., along the fibril axis.

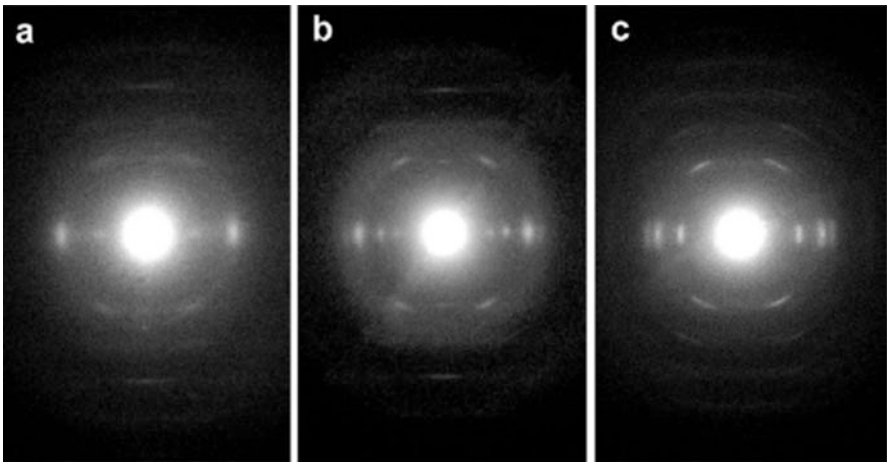

Fig. 9 Electron diffraction patterns on selected thin fibrillar areas of chitosan nanofibrils: (**a**) initially as originating from chitin heterogeneous deacetylation; (**b**) obtained after single acid hydrolysis of the chitosan sample in (**a**); (**c**) obtained after multistep acid hydrolysis of (**a**). The fiber axis is vertical. The fiber diffraction patterns in (**a**) and (**c**) correspond to the chitosan hydrated and anhydrous allomorphs, respectively, whereas that in (**b**) shows a mixture of both allomorphs [27]

Thermal Properties

The thermal stability of polysaccharide nanofibers is critical for further processing into nanocomposites. Due to the highly crystalline structure, good thermal stability of polysaccharide nanofibers would be expected, which should be better than that of the native substrate. However, it seems that the processing conditions might have an important influence on the final thermostability. For the original cellulose samples, it was observed that the thermal decomposition temperature shifted to higher values with increasing crystallite size, although the activation energy for thermal degradation remained almost constant [52]. The cellulose nanocrystals obtained after acid hydrolysis using hydrochloric acid generally showed a decrease in thermal stability in relation to the original cellulose source, in parallel with the decreasing of the degree of polymerization, which can be ascribed to a higher number of reducing polymer chain ends [53]. The complex behavior during decomposition of sulfated nanocellulose contains multiple steps that correspond to different degradation processes, i.e., hydrolysis of the outer sulfated cellulose, char formation and decomposition of amorphous traces, and finally dehydration and depolymerization [54].

The thermal stability of cellulose nanowhiskers decreases with the content of sulfate ester groups. Thermogravimetric analysis (TGA) diagrams of whiskers obtained by a water-mediated ionic liquid (IL) treatment exhibited significant differences compared to that of the original cellulose substrate, namely, microcrystalline cellulose (MCC) [19]. The MCC only presents a one-step degradation in the 300–400 °C temperature range, while the whiskers after IL treatment experienced a two-step degradation profile. The first degradation phase at 200–300 °C exhibited a

maximum degradation rate at 285 ± 1 °C, and the second degradation phase at 300 and 400 °C reaches its maximum rate at 346 ± 2 °C. A two-stage degradation process is in line with the thermal behavior reported for whiskers prepared using concentrated sulfuric acid as well, with the notable difference that thermal degradation starts at much higher temperature for IL-derived whiskers. It is observed that the whiskers obtained by a treatment in aqueous/IL environment are thermally more stable than the whiskers prepared under conditions of concentrated sulfuric acid. The whiskers from bacterial cellulose show the first degradation temperature between 226 and 262 °C, which is 25–60 °C lower than in the water/IL method [54]. It can be considered that the first degradation stage is related to the amorphous and esterified cellulose fraction and the higher thermal stability for IL-derived whiskers is consequently related to the smaller amount of surface derivatization in line with lower sulfur content in the material. In addition, the second degradation temperature for the IL-derived whiskers is much higher (346 ± 2 °C) than the degradation temperatures for bacterial cellulose nanowhiskers (250–300 °C).

However, when the polymer chain ends are acetylated, thermal stabilization occurs mainly due to the protection of the surface OH groups by the more stable acetyl groups. As the presence of sulfate groups reduces the thermal stability of the cellulose nanocrystals, routes have been developed to improve the thermal stability either by diminishing the sulfate groups by desulfation or neutralizing them by using NaOH solution [55]. The posttreatment with alkali or functionalization of the surface of cellulose nanowhiskers might therefore be a way to restore the thermal stability. In general, the thermal stability of the polysaccharide nanocrystals varies as a function of the acid strength and processing conditions [56].

Also for the fibrillated cellulose materials, the thermal stability is highly determined by the surface properties. The creation of a high surface area after fibrillation may be a reason for early thermal degradation by possible oxidation. The variations in thermal degradation behavior depending on the number of processing steps during fibrillation have been noticed: in general, a decrease in thermal stability can be attributed to the degradation of the cellulose under friction. However, a non-monotonous decrease in thermal stability may be attributed to the reorientation of the chemical components and/or a high possibility of lignin and hemicellulose degradation that favored catalytic behavior [57]. The thermal stability of nanofibrils with a high amount of residual lignin is significantly higher than that for CNF with low lignin contents, and the maximum rate of degradation occurring at 390 °C is among the highest reported value [58].

Rheological Properties

The rheological behavior of polysaccharide nanofibers in aqueous media comprises a complex study of particles in colloidal suspensions. The rheological properties are mostly controlled by the dimensions and surface charges of the nanofiber. The whiskers and fibrillated nanofibers can be described as nonspherical particles, and the viscosity of their suspensions strongly depends on the morphology. It can

generally be assumed that the viscosity of suspensions will increase for the particles with the higher aspect ratio and the viscosity values are much higher compared to the values for spherical particles. The probability of interaction and entanglement between fibers with high aspect ratio likely increases and causes an increase in viscosity, because it can be assumed that the fibrils become more "flexible." The viscosity of an aqueous nanocellulose dispersion can directly be expressed as a function of the aspect ratio, as shown in Fig. 10 [59].

For crystalline particles (CNWs), the suspensions behave mostly as a liquid with low viscosity and easy flow. As a result, the orientation of short rodlike particles at higher shear rates leads to shear thinning effects under permanent shear flow. In particular, the rheological properties of suspensions with nonspherical particles of high aspect ratio are largely controlled by the orientation of the particles under certain flow conditions, which are determined by the action of hydrodynamic forces. Although the nanofiber suspensions have relatively high viscosity at rest, they start to flow more easily under shear as the fiber network breaks down and the viscosity decreases. The instabilities in the nanofiber suspensions under a given shear conditions may occur through the flocculation and aggregation initiated by the interparticle interactions, depending on the fiber morphology or the degree of fibrillation. The particle interactions result in a liquid-like behavior with shear thinning effects under low fiber concentrations, while gel formation happens at higher fiber concentrations: e.g., the gelling properties of semi-dilute CNW suspensions occurred at concentrations of 0.2–0.3 vol. % [60]. The strong tendency for the formation of a fiber network from micro- and nanofibrils already occurs after processing at even low concentrations and causes a gel-like behavior of the suspension with the occurrence of a yield stress and elastic behavior only at very low concentrations of around 0.1%. The yield stress and yield strain of the gels vary with the strength, the particle shapes, and their mutual interactions. Indeed, the microfibrillated networks require a relatively high force to start flowing. As a consequence, the high yield stress favors the use of fibrillated celluloses as stabilizer for suspensions or emulsions as particles or droplets become easily trapped within the network and prevent them from sinking or floating. Depending on the degree of fibrillation, the viscosity increased with higher amount of fibrillation, but intermediate plateau

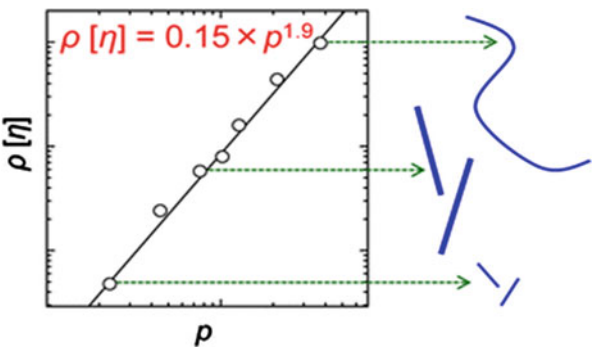

Fig. 10 Relation between intrinsic viscosity [η] and density ρ for suspensions of nanocellulose fibers with aspect ratio p [59]

values are characteristic for temporary aggregation and breaking up of the fiber network. Therefore, optimum processing conditions of the MFC/NFC suspensions should provide optimum fiber network morphology with smooth rheological characteristics. The interactions at fibrillar level may induce a "memory" or "time-dependent" effects in the fiber suspension with retarded recovery of the deformation state [61]. The dynamic yield point measured at a specific strain as a measure for the transition from the gel-like to the liquid-like regime does not depend on the conditions of processing [38]. However, it remains difficult to relate the processing conditions for fibrillated cellulose in a microfluidizer and resulting morphology to the rheological properties. When considering a group of rheological parameters as the rotational Péclet number (Pe), the higher number of passes during processing interestingly causes a progressive increase in Pe. Therefore, the latter parameter Pe can serve as a unique parameter for the selection of rheological properties of an MFC suspension in relation with its processing conditions and morphology (Fig. 11) [38]. Based on this value, the processing parameters for fibrillated cellulose suspensions can be adapted toward specifically required rheological properties.

A mechanism for gelation is attributed to the formation of physical entanglements between the nanofibers in result of their high surface area and high aspect ratio. As a result, hydrogels of chitin have been formed by chitin nanocrystals with the storage modulus reaching 169 kPa at 13% chitin content [62]. Alternatively, gels from chitin nanofibers have been developed where the gelation is induced by neutralization of the charged suspension so that electrostatic repulsion effects are removed, inducing precipitation and secondary bond interaction between nanofibers [63]. It is evident

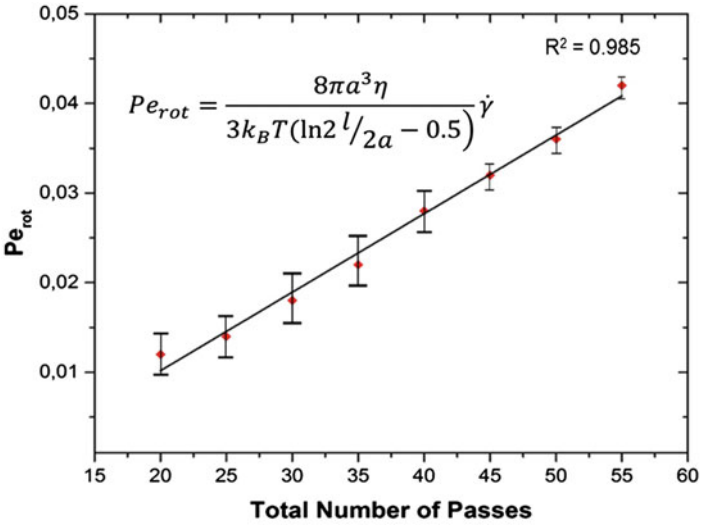

Fig. 11 Relation between rheological properties (rotational Péclet number) and processing conditions for fibrillated cellulose in a microfluidizer with increasing number of passes, with a, fiber diameter; l, fiber length; k_BT, thermal energy; η, viscosity; γ, shear rate [38]

that the nanofiber surface interactions are controlled by the present surface charges and indirectly by the pH, as the higher pH induces more repulsion charges and causes a gradual decrease in viscosity [64]. Practically, the highly crystalline hydrogels from α-chitin nanofibers can be prepared by a simple NaOH treatment at low temperatures, or mild conditions can be applied to both α-chitin powder and nanofibers to make hydrogels using calcium chloride dehydrate-saturated methanol, while nanofibrillation of the powder occurs during the treatment [65].

Mechanical Properties

The mechanical properties of single CNWs are very difficult to determine and cannot be uniquely assigned. After removal of the amorphous states of native cellulose fibers by acid hydrolysis, the remaining nanowhiskers should theoretically have a modulus close to a defect-free cellulose crystal. According to experimental AFM bending stiffness measurements on a single CNW from tunicate with cross-sectional diameters of 8–20 nm, the elastic moduli were measured for single microfibrils from TEMPO oxidation (145.2 ± 31.3 GPa) and acid hydrolysis (150.7 ± 28.8 GPa), respectively. The experimentally determined modulus was in agreement with the elastic modulus of native cellulose crystals, and values represent a good approximation to the crystalline cellulose [66]. The other measurements by Raman spectroscopy provided similar values for stiffness of about 143 GPa [67]. Experimental measurements of the CNW modulus with the use of sound velocities by inelastic X-ray scattering yielded a value of 15–220 GPa [68], which is much higher than theoretical estimates in the range of 100–160 GPa [69], due to influences of molecular dynamics/mechanics, ordered/disordered states and anisotropy. However, it is doubtful that the mechanical properties and stiffness of nanofibers extracted from biomass would approximate the modulus of crystalline cellulose. In the internal structure within the nanofibrils, whisker nanocrystals will have those properties while the experimental values for the nanofibers may be variable. The latter can only be assessed by good understanding of the arrangements and interactions of the sub-nanofibril fiber structures [69]. The moduli of nanofibrils within MFC sheets were about 29–36 GPa based on Raman spectroscopy and are within the same range of moduli for intact plant fibers. However, the experimental elastic modulus of MFC films prepared from softwood pulp after high-pressure homogenization reached up to 6.7 GPa with a tensile strength of 105 MPa, while the MFC films from hardwood pulp have elastic modulus of 6.3 GPa and tensile strength of 92 MPa [70]. The latter strongly depend on the preparation conditions and degree of fibrillation, as the MFC films prepared by an enzymatic pretreatment and mechanical fibrillation from softwood pulp show elastic moduli of around 10.4–13.7 MPa and tensile strength of 129–214 MPa, yielding nanopaper structures with extremely high toughness [71].

Otherwise, the bacterial cellulose fibrils have a modulus of 79–88 GPa as determined by Raman spectroscopy and are comparable to values reported from measurements by AFM cantilever approach [72]. It seems therefore that the mechanical properties of nanofibers extracted from the cell wall of plants or bacterial

cellulose strongly differ from the properties of cellulose nanocrystals. The variations in mechanical properties strongly relate to the internal state of order of the nanofibers and fibrils, including the orientation of molecular chains along the fibril axis and as an indirect consequence the degree of crystallinity, as proven by studies on the degree of disordered material in cellulose nanocrystals [73]. The variation in degree of crystallinity for cellulose nanofibers is reflected in the different mechanical properties [17]: the cellulose chains are tightly packed into crystallites that are stabilized by a strong and very complex intra- and intermolecular hydrogen bond network within the crystalline regions. Therefore, the strength and modulus of nanofiber film from wood, rice straw and potato tuber prepared by mechanical methods were around 210–230 MPa and 11 GPa, respectively, with the degree of crystallinity around 76–80% [74]. Otherwise, an improvement in mechanical properties of nanowhisker films has been observed after elimination of the sulfate groups from the cellulose nanowhiskers after neutralization. The charged sulfate groups result in stable suspension of cellulose nanowhiskers due to electrostatic repulsion. The elimination of surface charge leads to the formation of strongly bound nanofibrils and good nanofibrillar interactions, while the presence of charges rather induces electrostatic repulsion forces [75].

The mechanical properties of individual chitin nanofibers have been calculated from measurements on dried films, depending on different drying methods of the corresponding nanofiber networks: a comparative value of the elasticity modulus $E = 5–7$ GPa was calculated for the different fibers indicating similar qualities of the individual fibers [76]. However the elastic modulus of individual fibers is higher than the elastic modulus of the bulk films due to the bending of fibers in an intertwined network. The presence of functional groups, in particular acetyl groups, on the chitin/chitosan nanocrystals contributes to the formation of a hydrogen bond network and stabilization of the crystalline structure: therefore, the higher degrees of acetylation lead to increasing stiffness and lower ductility of the fibers in parallel with the better resistance against fracture as demonstrated at the atomistic level [77]. By using a special chemical route without chemical etching for the disintegration of the chitin nanofibrils, the hierarchical internal structure of chitin nanofibers resulting from the self-assembly in a chiral nematic phase could be preserved, and exceptional mechanical properties can be preserved in order to simulate their natural occurrence [78] with observed changes in the load bearing capacity, according to the conformation of chiral order. The presence of surface charges clearly affects the mechanical properties, as the hydrogels of partially deacetylated α-chitin nanofibers (positive charges) present higher storage moduli than the values for TEMPO-oxidized α-chitin nanofibers (negative charges) [79]. These were mainly explained by the presence of longer chitin nanofibers/nanowhiskers with a higher aspect ratio in positive correlation with the elasticity of the hydrogel without the presence of any cross-linking agent. In the hydrogel system of chitin nanofibers, water is an important factor that restricts the destruction of chitin crystalline structures caused by calcium ions; therefore, a mild method for the production of a hydrogel with highly crystalline α-chitin nanofibers was developed with high tensile properties under wet strength conditions [65]. The tensile strength for chitin hydrogels obtained from

20 wt% NaOH solutions (1.8 MPa) and Ca solvent (1.3 MPa), respectively, was relatively high in the wet state, unlike the properties for conventional regenerated hydrogels.

The stiffness of individual nanowhiskers could also be determined by theoretical models after dispersing them into a polymer matrix, by following the local molecular deformation of the whiskers using Raman spectroscopy. As such, the mechanical properties of different types of single nanofibers, fibrils and whiskers, were calculated from a back-calculation of the overall properties of a polymer composite [80]. The elastic properties of the fillers were determined from a multiscale model, yielding an approximation of the effective longitudinal Young's modulus of the fibrils of 65 GPa for nanofibrillated cellulose, 61 GPa for cellulose nanowhiskers and only 38 GPa for the microcrystalline cellulose. This agrees with other studies on nanoscale morphology and stiffness estimates of the single nanofiber. In particular, the effects of debonding, matrix yielding, and buckling of single whiskers were demonstrated and play a key role in the reinforcing action of CNW fillers. Besides the effects of interface compatibility, the formation of a percolation network structure of the nanofibers within a nanocomposite material predominantly explains the reinforcing action of nanowhiskers. The formation of a stiff three-dimensional organization of nanowhiskers in a continuous network establishes at concentrations above a percolation threshold value, depending on the aspect ratio of the nanowhiskers. As such, the fibers with higher aspect ratios ensure a better percolation with improved mechanical properties at the lower fiber loads.

Emerging Applications in High-Performance Nanocomposites

High Mechanical Performance Nanocomposites

The polysaccharide nanofibers have been introduced as mechanical reinforcement for both thermoplastic and thermoset polymer matrices. In relation with the excellent mechanical properties of the whisker nanocrystals, they can improve strength and stiffness of nanocomposites. In fact, the elastic modulus and tensile strength for cellulose nanocomposites scale linearly with the mechanical properties of cellulose nanopaper structures [81]. However, a good dispersion of the polysaccharide nanofibers in the polymer matrix remains a critical parameter. Again, the effects of debonding, matrix yielding and buckling of single nanocrystals were demonstrated. They play a key role in the reinforcing capacity of nanocrystal fillers [82]. Besides the effects of fiber/matrix interface compatibility, the formation of a percolation network structure of the nanofibers within the matrix predominantly explains the nanowhisker reinforcing action. For higher fiber contents, the strong whisker/whisker interactions and the percolation effect explain the high values of the rubber module of the composites [83]. These interactions occur by means of hydrogen bonds, which are established during the solvent evaporation in the composite processing. The formation of a stiff three-dimensional organization of whiskers like a continuous percolating network establishes at concentrations above a

percolation threshold. Such percolation effect can be analyzed according to the Halpin-Kardos mechanical model, including the elastic modulus of nanocomposites with various volume fractions of the reinforcing whiskers [84]. The percolation threshold depends on the aspect ratio (length/width: L/d) of the nanowhiskers and its spatial orientation according to the relation $v_{Rc} = 0.7 \cdot (L/d)^{-1}$. For example for chitin whiskers of *Riftia* tubes with a very high L/d (~120), the value of v_{Rc} is relatively low, e.g., 0.58% v/v [85]. The fibers with higher aspect ratios ensure a better percolation with improved mechanical properties at lower fiber loads. The stress transfer in the composite is then facilitated by the strong interactions in the whisker network above the threshold value V_{Rc} (Fig. 12). In addition to the drastic increase in the rubber module of the matrix due to the formation of a network of whiskers for contents higher than the percolation threshold, a stabilization of its value over a wider range of temperatures (rubber plateau) is also observed [86]. This rigid percolating network of whiskers is preferably formed for nanocomposite films processed by solvent evaporation [86]. The evaporation is a slow step giving sufficient time and mobility to the whiskers to establish hydrogen bonds and a rigid network in the matrix. In freeze-drying processings, the mobility of the matrix chains and the interaction of the whiskers are limited by the initial quenching. The different modes of stress transfer depend on fiber morphologies and surface properties. The interfacial energy dissipation at the interface between the polysaccharide nanocrystals and the matrix can be assessed from local micromechanical models providing a quantitative measure of the interface quality [87].

For thermoplastic matrices, for example, in polypropylene, the CNWs induced higher tensile strength in parallel with an increase in crystallinity of about 50% and

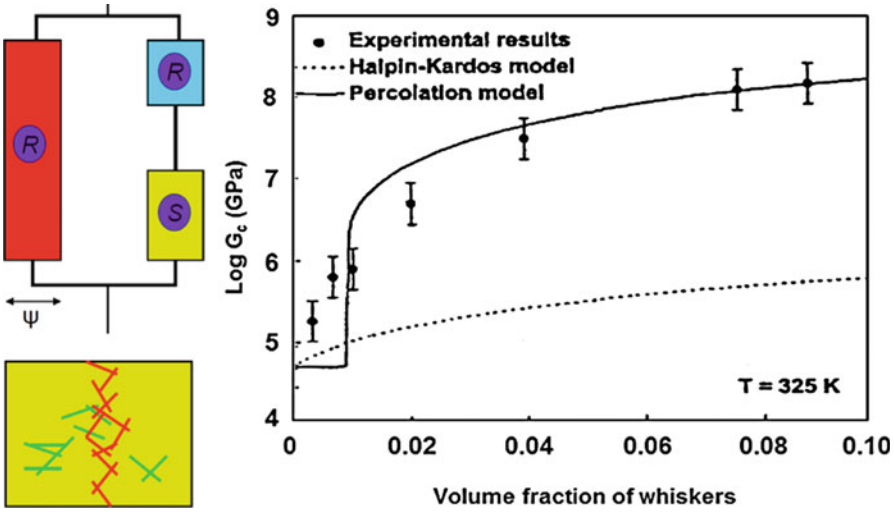

Fig. 12 Effect of reinforcement by nanowhiskers in a polymer matrix, (**a**) schematic representation of the threshold model, (**b**) influence of the formation of a percolation network on the mechanical properties [88]

higher thermal degradation temperature. To enhance the uniform distribution of CNWs in the composite, the polymer matrix can be dissolved in suitable solvent in combination with sonification and magnetic stirring [89]. The presence of CNWs generally increases the crystallinity of the polymer matrix, as it acts as a nucleating agent promoting crystallization. In most cases, however, the use of surface-modified CNW (e.g., silylated CNW) and plasticizers has been shown to enhance dispersion and minimize agglomerations [90]. Surface modification of the CNW to overcome the hydrophilicity is an important step to improve the compatibility and homogenous distribution of whiskers. The mechanical reinforcement effects of microfibrillated cellulose have been also studied for matrices like PLA [91], polyolefins, and polyurethane [92]. In general, the incorporation of a continuous and dense fibrillar network results in a linear increase in modulus, tensile strength and strain at fracture of polymer matrices, with key benefits on toughness improvement. Alternative to the surface modification, the in situ polymerization of thermoplastic polyurethane (TPU) in the presence of MFC was considered as a route for adequate MFC dispersion and network formation in the TPU matrix with strong interfacial interaction, resulting in significantly improved mechanical properties and thermostability [92]. For thermosets, the presence of CNW influences the curing behavior of epoxy resins, leading to the higher storage modulus of epoxy nanocomposites with the increase of CNW content [93]. In particular, the incorporation of CNWs could cause microphase separation and destroy the compactness of the matrix, which leads to the lowering of glass transition temperature (Tg). Nevertheless, some studies have revealed that the Tg was not significantly influenced by the incorporation of the cellulose filler. The improvements in mechanical performance of CNW-filled composites relies on the reinforcement of the matrix due to the formation and increase of interfacial interaction by hydrogen bonds between CNW nanofiller and the epoxy matrix [94]. The use of CNW in combination with a two-component waterborne polyurethane resulted in higher tensile strength and elastic modulus, in parallel with the increase in α-relaxation temperature and Tg due to the formation of a rigid CNW nanophase acting as cross-linking points within the matrix [95]. Finally, the addition of polysaccharide nanocrystals significantly enhances the mechanical performance of nanocomposites [86]. This effect depends on composite processing parameters, the nanofiber origin and consequently their chemical nature and aspect ratio L/d [83, 86].

Nanocomposites of Improved Thermal Properties

It is well established that the thermal properties of polymers, viz., Tg and melting temperature (Tm), but also the thermal stability and viscoelastic properties upon heating can be influenced by the addition of fibers [96]. The efficiency of fiber additives highly depends on the compatibility with the surrounding polymer matrix and local interface interactions [97]. The macroscopic performances of nanocomposites, in particular mechanical, barrier and biodegradation properties are strongly influenced by the thermal properties [98]. In composites, the main thermal transitions of a polymer matrix, Tg for an amorphous phase and Tm and Tc

(crystallization temperature) for a crystalline phase, reflect the morphologies of both the matrix and the matrix/fiber interphases [99]. The impact of polysaccharide nanofibers on the main thermal transitions of polymers including Tg, Tm and Tc was reviewed by Osorio-Madrazo et al. [100]. The literature mainly reports on polysaccharide nanofiber-filled nanocomposites with thermoplastic semicrystalline polymer matrices. The role of nanofiber surface attributes (surface chemistry and area), shape (whisker nanocrystals or nanofibril networks) and loading amount on thermal properties of the resulting composites has been investigated. Among others, the behavior of biopolymer matrices in particular of biodegradable polymers like poly(hydroxyalkanoates) (PHAs), poly(lactic acid) (PLA) polycaprolactone (PCL), and poly(ethylene oxide) (PEO) has been studied.

When a rigid filler like the native crystalline polysaccharide nanofibers is dispersed into and molecularly bonded with a polymer matrix, an increase and broadening of the Tg are observed in relation to the intensity of fiber/matrix interactions [96]. Stiff fibers are expected to constrain main matrix chain motions as well as induce heterogeneity due to concentration fluctuations together with possible attractive interactions. The shift in Tg and Tm in polymer blends with respect to the pure polymers reveals the morphology of the amorphous and crystalline phases, respectively. For example, the morphology and thermal properties of cellulose nanofiber/PHA nanocomposites have been one of the first systems studied in the literature. For PHA matrices, the Tg was not affected by the CNWs although the overall damping decreased with higher CNW loading, indicating the reduced mobility of the amorphous polymer chains [101]. In CNW/poly(3-hydroxybutyrate-co-3-hydroxyvalerate) (PHBV) composites, Tc was found to decrease with increasing CNWs, suggesting that CNWs have a nucleating effect on PHBV. Different studies have identified the dual effect of polysaccharide nanowhiskers as heterogeneous nucleating agents and as confinement [101]. It emerged from different studies that fiber loading plays a major role on the morphology and improvement of the thermal properties of PLA-based composites [102, 103]. While with differential scanning calorimetry (DSC) the Tg was not discernible in more crystalline composite samples, dynamic mechanical analysis (DMA) suggested a slight increase of Tg with the MFC loading in PLLA matrices [104]. MFC can facilitate and augment PLA crystallization, i.e., serves as a nucleating agent in addition to slightly rigidifying the amorphous phase.

Siqueira et al. [105] engaged in comparing the impact of the two main types of polysaccharide nanofibers, i.e., nanowhiskers and nanofibril networks on the properties of the resulting nanocomposite thermal properties. Polycaprolactone (PCL) was filled with different nanofiber amounts (3, 6, 9, and 12% of CNWs or MFCs) [105]. For all samples, the Tg significantly increased, indicating reduced chain mobility in the amorphous phase of PCL in the presence of nanofibers. Crystallinity also increased in all nanocomposites as well as the Tc value, indicating facilitated crystallization and stiffer resulting materials. The synergistic effects of surface chemistry, surface area and chain mobility on the thermal properties of nanocomposites were systematically studied by altering the interfacial properties and modification of the nanocomposites with 9 wt% of C18-modified fibers. Typically,

the broadening and occurrence of multiple endothermic melting peaks in DSC scans have been observed during isothermal crystallization experiments. This double melting peak has been assigned to the coexistence of spherulites and a trans-crystalline layer with lower crystal perfection developing at the surface of the polysaccharide nanofibers [105]. Together with the higher crystallinity, a depression of equilibrium melting point has been observed. This is ascribed to the nucleating effect of the nanofibers, with their magnitude directly related to the fiber surface area and aspect ratio. As for PLA composites, isothermal crystallization studies of PCL composites with high filler loadings demonstrated that polysaccharide nanofibers expedited the polymer matrix crystallization and slightly more with the MFC than with the nanowhiskers [105].

Summarizing, the thermal properties of polysaccharide nanofiber-filled composites depend on composition and microstructure as well as on filler loading and fiber/matrix compatibility. The loading, the surface and interfacial areas, and the surface chemistry of the polysaccharide nanofibers play an important role in the morphology and resulting thermal properties of the nanocomposites.

Conclusion

Owing to the unique occurrence of cellulose and chitin polysaccharide materials, their structural organization and specially their native directional packing, forming highly crystalline fibers in a variety of natural sources, they can be processed into crystalline nanofibers. It is evident that a good understanding of the crystalline structure of these materials is crucial to define the optimum processing conditions. Then, the native properties of the crystalline polysaccharide fibers significantly influence the morphology and properties of the obtained nanofibers. The chemical and mechanical processing routes to obtain the latter also require to be optimized. In particular, the high energy demands should be covered by developing appropriate pretreatment of the available biomass. The intrinsic properties of the nanofibers such as morphology, crystalline microstructure, thermal properties, rheology and mechanical properties can be well controlled by a strict definition of the processing steps. In further considerations, the particular use of the nanofibers in nanocomposite formulations is of great interest nowadays. In one hand, for the mechanical reinforcing capacity, two prerequisites to be considered are the control over the percolation network threshold for favorable interactions between the nanofibers, and the eventual surface modification for good interactions at the interface between the fibers and composite matrix. On the other hand, the survey of particular polymers/polysaccharide nanofiber composites has clearly shown the significant impact of these fibers on the overall thermal properties of composites, with thermal stabilization occurring especially in low modulus matrices (amorphous in the rubbery states and above Tm for semicrystalline polymers). Depending on the phase state of the polymer matrix and the competition between nanofiber/nanofiber and nanofiber/matrix interactions, thermal stabilization might be also described with the percolation network model as for the mechanical performance of the composites.

References

1. Sugiyama J, Harada H, Fujiyoshi Y, Uyeda N (1985) Lattice images from ultrathin sections of cellulose microfibrils in the cell wall of Valonia macrophysa Kütz. Planta 166:161–168
2. Nishiyama Y, Langan P, Chanzy H (2003) Preparation of tunicin cellulose Iβ samples for X-ray and neutron diffraction. Fibre Diffract Rev 11:75–78
3. Sugiyama J, Vuong R, Chanzy H (1991) Electron diffraction study on the two crystalline phases occurring in native cellulose from an algal cell wall. Macromolecules 24:4168–4175
4. Nishiyama Y, Lagan P, Chanzy H (2002) Crystal structure and hydrogen bonding system in cellulose Iβ from synchrotron X-ray and neutron fiber diffraction. J Am Chem Soc 124:9074–9082
5. Nishiyama Y, Johnson GP, French AD, Forsyth VT, Langan P (2008) Neutron crystallography, molecular dynamics, and quantum mechanics studies of the nature of hydrogen bonding in cellulose Iβ. Biomacromolecules 9:3133–3140
6. Nishiyama Y, Sugiyama J, Chanzy H, Langan P (2003) Crystal structure and hydrogen bonding system in cellulose Iα from synchrotron X-ray and neutron fiber diffraction. J Am Chem Soc 125(47):14300–14306
7. Chrétiennot-Dinet M-J, Giraud-Guille M-M, Vaulot D, Putaux J-L, Saito Y, Chanzy H (1997) The chitinous nature of filaments ejected by phaeocystis (Prymnesiophyceae). J Phycol 33:666–672
8. Blackwell J, Weih MA (1984) The structure of chitin-protein complexes. In: Zikakis JP (ed) Chitin, chitosan and related enzymes. Academic, London, pp 257–263
9. Neville AC (1993) Biology of fibrous composites; development beyond the cell membrane. Cambridge University Press, New York
10. Revol JF, Marchessault RH (1993) In vitro chiral nematic ordering of chitin crystallites. Int J Biol Macromol 15:329–335
11. Giraud-Guille M-M (1984) Fine structure of the chitin-protein system in the crab cuticle. Tissue Cell 16:75–92
12. Klemm D, Kramer F, Moritz S, Lindström T, Ankerfors M, Gray D, Dorris A (2011) Nanocelluloses: a new family of nature-based materials. Angew Chem Int Ed 50:5438–5466
13. Marchessault RH, Morehead FF, Walter NM (1959) Liquid crystal systems from fibrillar polysaccharides. Nature 184:632–633
14. Elazzouzi-Hafraoui S, Nishiyama Y, Putaux J-L, Heux L, Dubreuil F, Rochas C (2007) The shape and size distribution of crystalline nanoparticles prepared by acid hydrolysis of native cellulose. Biomacromolecules 9:57–65
15. Dufresne A (2012) Nanocellulose, from nature to high performance tailored materials. Berlin, Boston: De Gruyter
16. Fan Y, Fukuzumi H, Saito T, Isogai A (2012) Comparative characterization of aqueous dispersions and cast films of different chitin nanowhiskers/nanofibers. Int J Biol Macromol 50:69–76
17. Habibi Y, Lucia LA, Rojas OJ (2010) Cellulose nanocrystals: chemistry, self-assembly, and applications. Chem Rev 110:3479–3500
18. Kaushik M, Fraschini C, Chauve G, Putaux J.-L, Moores A (2015) Transmission electron microscopy for the characterization of cellulose nanocrystals. In: Maaz K (ed) The transmission electron microscope – theory and applications. InTech, London, pp 129–163
19. Mao J, Osorio-Madrazo A, Laborie M-P (2013) Preparation of cellulose I nanowhiskers with a mildly acidic aqueous ionic liquid: reaction efficiency and whiskers attributes. Cellulose 20:1829–1840
20. Abushammala H, Krossing I, Laborie M-P (2015) Ionic liquid-mediated technology to produce cellulose nanocrystals directly from wood. Carbohydr Polym 134:609–616
21. Abushammala H, Goldsztayn R, Leao A, Laborie M-P (2016) Combining steam explosion with 1-ethyl-3-methylimidazlium acetate treatment of wood yields lignin-coated cellulose nanocrystals of high aspect ratio. Cellulose 23:1813–1823

22. Fragal EH, Fragal VH, Huang X, Martins AC, Cellet TSP, Pereira GM, Mikmekova E, Rubira AF, Silva R, Asefa T (2017) From ionic liquid-modified cellulose nanowhiskers to highly active metal-free nanostructured carbon catalysts for the hydrazine oxidation reaction. J Mater Chem A 5:1066–1077
23. Osorio-Madrazo A, David L, Trombotto S, Lucas J-M, Peniche-Covas C, Domard A (2010) Kinetics study of the solid-state acid hydrolysis of chitosan: evolution of the crystallinity and macromolecular structure. Biomacromolecules 11:1376–1386
24. Watthanaphanit A, Supaphol P, Tamura H, Tokura S, Rujiravanit R (2010) Wet-spun alginate/chitosan whiskers nanocomposite fibers: preparation, characterization and release characteristic of the whiskers. Carbohydr Polym 79:738–746
25. Osorio-Madrazo A, Eder M, Rueggeberg M, Pandey J, Harrington MJ, Nishiyama Y, Putaux J-L, Rochas C, Burgert I (2012) Reorientation of cellulose nanowhiskers in agarose hydrogels under tensile loading. Biomacromolecules 13:850–856
26. Belamie E, Domard A, Chanzy H, Giraud-Guille MM (1999) Spherulitic crystallization of chitosan oligomers. Langmuir 15:1549–1555
27. Osorio-Madrazo A, David L, Peniche-Covas C, Rochas C, Putaux J-L, Trombotto S, Alcouffe P, Domard A (2015) Fine microstructure of processed chitosan nanofibril networks preserving directional packing and high molecular weight. Carbohydr Polym 131:1–8
28. Chakraborty A, Sain M, Kortschot M (2005) Cellulose microfibrils: a novel method of preparation using high shear refining and cryocrushing. Holzforschung 59:102
29. Kumar V, Bollström R, Yang A, Chen Q, Chen G, Salminen P, Bousfield D, Toivakka M (2014) Comparison of nano- and microfibrillated cellulose films. Cellulose 21:3443–3456
30. Spence KL, Venditti RA, Rojas OJ, Habibi Y, Pawlak JJ (2011) A comparative study of energy consumption and physical properties of microfibrillated cellulose produced by different processing methods. Cellulose 18:1097–1111
31. Ifuku S (2014) Chitin and chitosan nanofibers: preparation and chemical modifications. Molecules 19:18367
32. Fan Y, Saito T, Isogai A (2008) Chitin nanocrystals prepared by TEMPO-mediated oxidation of α-chitin. Biomacromolecules 9:192–198
33. Ifuku S, Nogi M, Abe K, Yoshioka M, Morimoto M, Saimoto H, Yano H (2011) Simple preparation method of chitin nanofibers with a uniform width of 10–20 nm from prawn shell under neutral conditions. Carbohydr Polym 84:762–764
34. Zhang Y, Jiang J, Liu L, Zheng K, Yu S, Fan Y (2015) Preparation, assessment, and comparison of α-chitin nano-fiber films with different surface charges. Nanoscale Res Lett 10(1):226
35. Janardhnan S, Sain M (2011) Targeted disruption of hydroxyl chemistry and crystallinity in natural fibers for the isolation of cellulose nano-fibers via enzymatic treatment. Bioresources 6(2):1242–1250
36. Cara C, Ruiz E, Ballesteros I, Negro MJ, Castro E (2006) Enhanced enzymatic hydrolysis of olive tree wood by steam explosion and alkaline peroxide delignification. Process Biochem 41:423–429
37. Xiong Y, Zhang Z, Wang X, Liu B, Lin J (2014) Hydrolysis of cellulose in ionic liquids catalyzed by a magnetically-recoverable solid acid catalyst. Chem Eng J 235:349–355
38. Taheri H, Samyn P (2016) Effect of homogenization (microfluidization) process parameters in mechanical production of micro- and nanofibrillated cellulose on its rheological and morphological properties. Cellulose 23(2):1221–1238
39. Schenzel K, Fischer S, Brendler E (2005) New method for determining the degree of cellulose I crystallinity by means of FT Raman spectroscopy. Cellulose 12(3):223–231
40. Saurabh CK, Mustapha A, Masri MM, Owolabi AF, Syakir MI, Dungani R, Paridah MT, Jawaid M, Abdul Khalil HPS (2016) Isolation and characterization of cellulose nanofibers from Gigantochloa scortechinii as a reinforcement material. J Nanomater 2016:8
41. Duchemin BCZ, Newman R, Staiger M (2007) Phase transformations in microcrystalline cellulose due to partial dissolution. Cellulose 14(4):311–320

42. Kondo T, Togawa E, Brown RM (2001) "Nematic ordered cellulose": a concept of glucan chain association. Biomacromolecules 2(4):1324–1330
43. Iwamoto S, Nakagaito AN, Yano H (2007) Nano-fibrillation of pulp fibers for the processing of transparent nanocomposites. Appl Phys A 89(2):461–466
44. Qing Y, Sabo R, Zhu JY, Agarwal U, Cai Z, Wu Y (2013) A comparative study of cellulose nanofibrils disintegrated via multiple processing approaches. Carbohydr Polym 97(1): 226–234
45. Nair SS, Zhu JY, Deng Y, Ragauskas AJ (2014) Characterization of cellulose nanofibrillation by micro grinding. J Nanopart Res. 2014 16(4):2349
46. Yuanita E, Pratama JN, Chalid M (2017) Preparation of micro fibrillated cellulose based on Arenga Pinnata "Ijuk" fibre for nucleating agent of polypropylene: characterization, optimization and feasibility study. Macromol Symp 371(1):61–68
47. Clark GL, Smith AF (1936) X-ray diffraction studies of chitin, chitosan, and derivatives. J Phys Chem 40(7):863–879
48. Okuyama K, Noguchi K, Miyazawa T, Yui T, Ogawa K (1997) Molecular and crystal structure of hydrated chitosan. Macromolecules 30(19):5849–5855
49. Ogawa K, Hirano S, Miyanishi T, Yui T, Watanabe T (1984) A new polymorph of chitosan. Macromolecules 17(4):973–975
50. Saito H, Tabeta R, Ogawa K (1987) High-resolution solid-state carbon-13 NMR study of chitosan and its salts with acids: conformational characterization of polymorphs and helical structures as viewed from the conformation-dependent carbon-13 chemical shifts. Macromolecules 20(10):2424–2430
51. Okuyama K, Noguchi K, Hanafusa Y, Osawa K, Ogawa K (1999) Structural study of anhydrous tendon chitosan obtained via chitosan/acetic acid complex. Int J Biol Macromol 26(4):285–293
52. Kim U-J, Eom SH, Wada M (2010) Thermal decomposition of native cellulose: influence on crystallite size. Polym Degrad Stab 95(5):778–781
53. Agustin MB, Nakatsubo F, Yano H (2016) The thermal stability of nanocellulose and its acetates with different degree of polymerization. Cellulose 23(1):451–464
54. Roman M, Winter WT (2004) Effect of sulfate groups from sulfuric acid hydrolysis on the thermal degradation behavior of bacterial cellulose. Biomacromolecules 5(5):1671–1677
55. Wang N, Ding E, Cheng R (2007) Thermal degradation behaviors of spherical cellulose nanocrystals with sulfate groups. Polymer 48(12):3486–3493
56. Kargarzadeh H, Ahmad I, Abdullah I, Dufresne A, Zainudin SY, Sheltami RM (2012) Effects of hydrolysis conditions on the morphology, crystallinity, and thermal stability of cellulose nanocrystals extracted from kenaf bast fibers. Cellulose 19(3):855–866
57. Lekha P, Mtibe A, Motaung TE, Andrew JE, Sitholè BB, Gibril M (2016) Effect of mechanical treatment on properties of cellulose nanofibrils produced from bleached hardwood and softwood pulps. Maderas Ciencia y tecnología 18:457–466
58. Nair SS, Yan N (2015) Effect of high residual lignin on the thermal stability of nanofibrils and its enhanced mechanical performance in aqueous environments. Cellulose 22(5):3137–3150
59. Tanaka R, Saito T, Hondo H, Isogai A (2015) Influence of flexibility and dimensions of nanocelluloses on the flow properties of their aqueous dispersions. Biomacromolecules 16 (7):2127–2131
60. Le Goff KJ, Gaillard C, Helbert W, Garnier C, Aubry T (2015) Rheological study of reinforcement of agarose hydrogels by cellulose nanowhiskers. Carbohydr Polym 116: 117–123
61. Iotti M, Gregersen ØW, Moe S, Lenes M (2011) Rheological studies of microfibrillar cellulose water dispersions. J Polym Environ 19(1):137–145
62. Araki J, Yamanaka Y, Ohkawa K (2012) Chitin-chitosan nanocomposite gels: reinforcement of chitosan hydrogels with rod-like chitin nanowhiskers. Polym J 44(7):713–717
63. Mushi NE, Kochumalayil J, Cervin NT, Zhou Q, Berglund LA (2016) Nanostructurally controlled hydrogel based on small-diameter native chitin nanofibers: preparation, structure, and properties. ChemSusChem 9(9):989–995

64. Pääkkö M, Ankerfors M, Kosonen H, Nykänen A, Ahola S, Österberg M, Ruokolainen J, Laine J, Larsson PT, Ikkala O et al (2007) Enzymatic hydrolysis combined with mechanical shearing and high-pressure homogenization for nanoscale cellulose fibrils and strong gels. Biomacromolecules 8(6):1934–1941
65. Chen C, Yano H, Li D, Abe K (2015) Preparation of high-strength α-chitin nanofiber-based hydrogels under mild conditions. Cellulose 22(4):2543–2550
66. Iwamoto S, Kai W, Isogai A, Iwata T (2009) Elastic modulus of single cellulose microfibrils from tunicate measured by atomic force microscopy. Biomacromolecules 10(9):2571–2576
67. Šturcová A, Davies GR, Eichhorn SJ (2005) Elastic modulus and stress-transfer properties of tunicate cellulose whiskers. Biomacromolecules 6(2):1055–1061
68. Diddens I, Murphy B, Krisch M, Müller M (2008) Anisotropic elastic properties of cellulose measured using inelastic X-ray scattering. Macromolecules 41(24):9755–9759
69. Eichhorn SJ (2012) Stiff as a board: perspectives on the crystalline modulus of cellulose. ACS Macro Lett 1(11):1237–1239
70. Spence KL, Venditti RA, Habibi Y, Rojas OJ, Pawlak JJ (2010) The effect of chemical composition on microfibrillar cellulose films from wood pulps: mechanical processing and physical properties. Bioresour Technol 101(15):5961–5968
71. Henriksson M, Berglund LA, Isaksson P, Lindström T, Nishino T (2008) Cellulose nanopaper structures of high toughness. Biomacromolecules 9(6):1579–1585
72. Tanpichai S, Quero F, Nogi M, Yano H, Young RJ, Lindström T, Sampson WW, Eichhorn SJ (2012) Effective young's modulus of bacterial and microfibrillated cellulose fibrils in fibrous networks. Biomacromolecules 13(5):1340–1349
73. Lemke CH, Dong RY, Michal CA, Hamad WY (2012) New insights into nano-crystalline cellulose structure and morphology based on solid-state NMR. Cellulose 19(5):1619–1629
74. Abe K, Yano H (2009) Comparison of the characteristics of cellulose microfibril aggregates of wood, rice straw and potato tuber. Cellulose 16(6):1017
75. Fahma F, Hori N, Iwamoto S, Iwata T, Takemura A (2016) Cellulose nanowhiskers from sugar palm fibers. Emirates J Food Agric 28:566–571
76. Hassanzadeh P, Sun W, de Silva JP, Jin J, Makhnejia K, Cross GLW, Rolandi M (2014) Mechanical properties of self-assembled chitin nanofiber networks. J Mater Chem B 2(17): 2461–2466
77. Cui J, Yu Z, Lau D (2016) Effect of acetyl group on mechanical properties of chitin/chitosan nanocrystal: a molecular dynamics study. Int J Mol Sci 17(1):61
78. Oh DX, Cha YJ, Nguyen H-L, Je HH, Jho YS, Hwang DS, Yoon DK (2016) Chiral nematic self-assembly of minimally surface damaged chitin nanofibrils and its load bearing functions. Sci Rep 6:23245
79. Liu L, Wang R, Yu J, Jiang J, Zheng K, Hu L, Wang Z, Fan Y (2016) Robust self-standing chitin nanofiber/nanowhisker hydrogels with designed surface charges and ultralow mass content via gas phase coagulation. Biomacromolecules 17(11):3773–3781
80. Josefsson G, Berthold F, Gamstedt EK (2014) Stiffness contribution of cellulose nanofibrils to composite materials. Int J Solids Struct 51(5):945–953
81. Lee K-Y, Aitomäki Y, Berglund LA, Oksman K, Bismarck A (2014) On the use of nano-cellulose as reinforcement in polymer matrix composites. Compos Sci Technol 105:15–27
82. Rusli R, Eichhorn tJ (2008) Determination of the stiffness of cellulose nanowhiskers and the fiber-matrix interface in a nanocomposite using Raman spectroscopy. Appl Phys Lett 93:033111
83. Favier V, Chanzy H, Cavaillé JY (1995) Polymer nanocomposites reinforced by cellulose whiskers. Macromolecules 28:6365–6367
84. Matos Ruiz M, Cavaillé JY, Dufresne A, Gérard JF, Graillat C (2000) Processing and characterization of new thermoset nanocomposites based on cellulose whiskers. Compos Interfaces 7(2):117–131
85. Morin A, Dufresne A (2002) Nanocomposites of chitin whiskers from Riftia tubes and poly (caprolactone). Macromolecules 35(6):2190–2199

86. Gopalan Nair K, Dufresne A (2003) Crab shell chitin whisker reinforced natural rubber nanocomposites. 2. Mechanical behavior. Biomacromolecules 4(3):666–674
87. Rafeadah R, Stephen JE (2011) Interfacial energy dissipation in a cellulose nanowhisker composite. Nanotechnology 22(32):325706
88. Favier V, Cavaille JY, Canova GR, Shrivastava SC (1997) Mechanical percolation in cellulose whisker nanocomposites. Polym Eng Sci 37(10):1732–1739
89. Bahar E, Ucar N, Onen A, Wang Y, Oksüz M, Ayaz O, Ucar M, Demir A (2012) Thermal and mechanical properties of polypropylene nanocomposite materials reinforced with cellulose nano whiskers. J Appl Polym Sci 125(4):2882–2889
90. Sullivan E, Moon R, Kalaitzidou K (2015) Processing and characterization of cellulose nanocrystals/polylactic acid nanocomposite films. Materials 8(12):5447
91. Suryanegara L, Nakagaito A, Yano H (2010) Thermo-mechanical properties of microfibrillated cellulose-reinforced partially crystallized PLA composites. Cellulose 17(4): 771–778
92. Yao X, Qi X, He Y, Tan D, Chen F, Fu Q (2014) Simultaneous reinforcing and toughening of polyurethane via grafting on the surface of microfibrillated cellulose. ACS Appl Mater Interfaces 6(4):2497–2507
93. Wu G-m, Liu D, Liu G-f, Chen J, Huo S-p, Kong Z-w (2015) Thermoset nanocomposites from waterborne bio-based epoxy resin and cellulose nanowhiskers. Carbohydr Polym 127:229–235
94. Liu H, Laborie M-PG (2011) Bio-based nanocomposites by in situ cure of phenolic prepolymers with cellulose whiskers. Cellulose 18(3):619–630
95. Wu G-M, Chen J, S-p H, G-f L, Kong Z-W (2014) Thermoset nanocomposites from two-component waterborne polyurethanes and cellulose whiskers. Carbohydr Polym 105:207–213
96. Ferry JD (1980) Viscoelastic properties of polymers. Wiley, New York
97. Utracki LA (ed) (2003) Polymer blends handbook. Kluwer Academic, Dordrecht
98. Kowalczyk M, Piorkowska E, Kulpinski P, Pracella M (2011) Mechanical and thermal properties of PLA composites with cellulose nanofibers and standard size fibers. Compos A: Appl Sci Manuf 42(10):1509–1514
99. Gedde UW (1995) Polymer physics. Chapman & Hall, London
100. Osorio-Madrazo A, Laborie M-P (2013) Morphological and thermal investigations of cellulosic bionanocomposites. In: Dufresne A, Thomas S, Pothen LA (eds) Biopolymer nanocomposites. Wiley, Hoboken, pp 411–436
101. Jiang L, Morelius E, Zhang J, Wolcott M, Holbery J (2008) Study of the poly (3-hydroxybutyrate-co-3-hydroxyvalerate)/cellulose nanowhisker composites prepared by solution casting and melt processing. J Compos Mater 42(24):2629–2645
102. Oksman K, Mathew AP, Bondeson D, Kvien I (2006) Manufacturing process of cellulose whiskers/polylactic acid nanocomposites. Compos Sci Technol 66(15):2776–2784
103. Suryanegara L, Nakagaito AN, Yano H (2009) The effect of crystallization of PLA on the thermal and mechanical properties of microfibrillated cellulose-reinforced PLA composites. Compos Sci Technol 69(7):1187–1192
104. Luiz de Paula E, Mano V, Pereira FV (2011) Influence of cellulose nanowhiskers on the hydrolytic degradation behavior of poly(d,l-lactide). Polym Degrad Stab 96(9):1631–1638
105. Siqueira G, Fraschini C, Bras J, Dufresne A, Prud'homme R, Laborie M-P (2011) Impact of the nature and shape of cellulosic nanoparticles on the isothermal crystallization kinetics of poly (ε-caprolactone). Eur Polym J 47(12):2216–2227